

# Electron transport and redox reactions in carbon-based molecular electronic junctions

Richard L. McCreery, Jing Wu and Rajendra Prasad Kalakodimi†

Received 24th January 2006, Accepted 7th April 2006

First published as an Advance Article on the web 4th May 2006

DOI: 10.1039/b601163m

A unique molecular junction design is described, consisting of a molecular mono- or multilayer oriented between a conducting carbon substrate and a metallic top contact. The  $sp^2$  hybridized graphitic carbon substrate (pyrolyzed photoresist film, PPF) is flat on the scale of the molecular dimensions, and the molecular layer is bonded to the substrate *via* diazonium ion reduction to yield a strong, conjugated C–C bond. Molecular junctions were completed by electron-beam deposition of copper, titanium oxide, or aluminium oxide followed by a final conducting layer of gold. Vibrational spectroscopy and XPS of completed junctions showed minimal damage to the molecular layer by metal deposition, although some electron transfer to the molecular layer resulted in partial reduction in some cases. Device yield was high (> 80%), and the standard deviations of junction electronic properties such as low voltage resistance were typically in the range of 10–20%. The resistance of PPF/molecule/Cu/Au junctions exhibited a strong dependence on the structure and thickness of the molecular layer, ranging from  $0.13 \Omega \text{ cm}^2$  for a nitrobiphenyl monolayer, to  $4.46 \Omega \text{ cm}^2$  for a biphenyl monolayer, and  $160 \Omega \text{ cm}^2$  for a 4.3 nm thick nitrobiphenyl multilayer. Junctions containing titanium or aluminium oxide had dramatically lower conductance than their PPF/molecule/Cu counterparts, with aluminium oxide junctions exhibiting essentially insulating behavior. However, *in situ* Raman spectroscopy of PPF/nitroazobenzene/ $\text{AlO}_x$ /Au junctions with partially transparent metal contacts revealed that redox reactions occurred under bias, with nitroazobenzene (NAB) reduction occurring when the PPF was biased negative relative to the Au. Similar redox reactions were observed in PPF/NAB/ $\text{TiO}_x$ /Au molecular junctions, but they were accompanied by major effects on electronic behavior, such as rectification and persistent conductance switching. Such switching was evident following polarization of PPF/molecule/ $\text{TiO}_2$ /Au junctions by positive or negative potential pulses, and the resulting conductance changes persisted for several minutes at room temperature. The “memory” effect implied by these observations is attributed to a combination of the molecular layer and the  $\text{TiO}_2$  properties, namely metastable “trapping” of electrons in the  $\text{TiO}_2$  when the Au is negatively biased.

## 1. Introduction

The term “molecular electronics” (ME) has been used to describe various electron transport (ET) phenomena of possibly significant fundamental and practical importance.<sup>1–4</sup> Compared to metallic conductors and doped semiconductors, ET in molecules is a conceptually distinct phenomenon, with a strong dependence on molecular orbitals, structure and bonding. The historical context of molecular electronics includes several ET phenomena which have been investigated extensively. ET in donor–bridge–acceptor (DBA) complexes is controlled by molecular structure and conformation,<sup>5–12</sup> and an early surprise was ET across  $40 \text{ \AA}$  of a DNA helix.<sup>13–15</sup> Since  $40 \text{ \AA}$  is normally considered too far for ET by coherent tunneling, questions rapidly arose about DNA as a “conduc-

tor”. ET through molecular monolayers on metal surfaces has been studied extensively by electrochemists in an experiment conceptually similar to replacing the donor or acceptor of a DBA complex with a conducting solid.<sup>16–21</sup> ET in conducting polymers has been investigated extensively, of course, and is generally classified into band transport, hopping (*i.e.* redox exchange), and a variety of other mechanisms.<sup>22–27</sup> Electronic devices such as organic light emitting diodes, thin film transistors and conducting polymers are generally classified as “organic electronics”, a broad designation of which ME could be considered a subset.<sup>28–35</sup>

Within the context of the rich history of ET in molecules, solids, and at electrode surfaces, the term “molecular electronics” is used in this report to describe ET phenomena with three characteristics. First, there is some degree of electronic coupling between a molecule and a traditional conductor or semiconductor.<sup>36–42</sup> Such coupling is necessary in order to “connect” the molecule or array of molecules to an integrated circuit, power source, *etc.* Second, at least one dimension in a ME device is small enough (usually 1–10 nm) that transport

Department of Chemistry, The Ohio State University, 100 W 18th Avenue, Columbus, OH 43210, USA. E-mail: mcreery.2@osu.edu; Tel: 614-292-2021

† Present address: General Electric, Bangalore, India.

phenomena may be fundamentally different from those observed in bulk materials. For example, coherent tunneling may be the dominant ET mechanism over a 1–2 nm dimension, but is not possible for typical “thin” films with > 10 nm thickness. Third, most ME paradigms involve oriented molecules, as opposed to the randomly oriented chains of most conducting polymers or polycrystalline solids. Such alignment permits phenomena such as rectification, which would not be expected for an amorphous or polycrystalline film. A single molecule suspended between two conducting contacts is one paradigm which fits these three characteristics, and is the basis of several ME investigations based on scanning probe microscopy (Fig. 1A).<sup>43–55</sup> Much of the early excitement about ME was the prospect of a single molecule acting as a single-bit memory, thus greatly increasing the potential device density in microelectronic circuits.<sup>56–61</sup> A molecular junction may also incorporate  $10^3$ – $10^{12}$  molecules oriented in parallel between conducting or semiconducting “contacts”, as shown in Fig. 1B.<sup>4,39,57,62,63</sup> Such junctions are one molecule thick but have cross sectional areas ranging from  $< 1 \mu\text{m}^2$  to  $\sim 1 \text{mm}^2$ .

We have used a distinct approach to investigating ET in molecular electronic junctions, which is based on a graphitic carbon substrate and covalent carbon–carbon bond between substrate and molecular monolayer.<sup>4,64–71</sup> Since the resulting junctions differ substantially from the alternative designs reported to date, the fabrication and structural characterization of carbon-based molecular junctions are addressed in some detail. Then the electronic behavior of such junctions is described, with particular attention to the effects of variations in molecular structure on junction conductance and hysteresis. Before considering junction fabrication, however, some comments about ET mechanisms are appropriate.

### 1.1 Electron transport in molecular junctions

A molecular junction can be considered to be one electronic system, consisting of two conducting or semiconducting solids bridged by a molecular layer. Specifically, we need to consider how an electron might be transmitted from one conventional conductor to another across a gap which may contain one or more oriented molecules. Since many ET mechanisms are strongly dependent on the distance between the conductors,

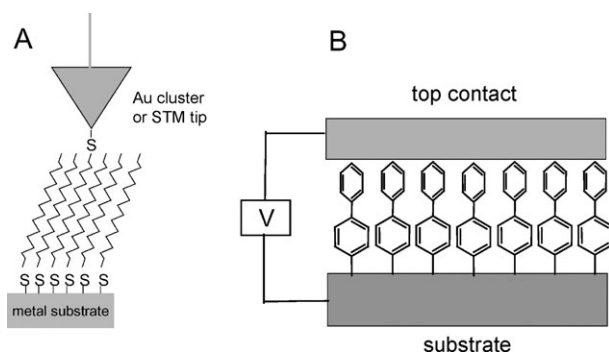


**Fig. 1** “Single molecule” (A) and “molecular junction” (B) paradigms for investigating electron transport through molecules positioned between two conducting contacts.

the short dimension noted earlier becomes particularly important. Fig. 2 illustrates a few of the many possible ET mechanisms, for the case of a molecular junction. A vacuum gap between two conductors can “conduct” when the gap is small enough to permit overlap of the electron wave functions in the conductors (Fig. 2A).<sup>72,73</sup> Stated differently, an electron in one conductor has a finite probability of being present in the other conductor as a consequence of coherent quantum mechanical tunneling. As noted in Table 1, the distance dependence of coherent tunneling through a vacuum is exponential and quite steep, with a tunneling barrier equal to the work function of the “source” conductor. A common parameter to describe the distance dependence is  $\beta$  (units of  $\text{\AA}^{-1}$ ), the absolute value of the slope of a plot of  $\ln(J)$  vs. the width of the gap, where  $J$  is the current density through the vacuum gap for a particular bias. For example, a  $\beta$  of  $1.0 \text{\AA}^{-1}$  indicates a decrease in tunneling current of a factor of  $1/e$  for each additional  $\text{\AA}$  of gap width. The parameter  $\beta$  is proportional to the square root of the tunneling barrier height, with  $\beta$  ranging from 2.0–2.3  $\text{\AA}^{-1}$  for typical work functions of 4–5 eV.<sup>72,73</sup> Given this steep exponential distance dependence, vacuum tunneling is very inefficient as the gap increases past  $\sim 15 \text{\AA}$ .

When a molecule is present in the tunneling gap (Fig. 2B), the tunneling rate may increase significantly due to several effects which are often labeled collectively as “superexchange”.<sup>20,74–79</sup> The orbitals and electrons in the gap can interact with the tunneling electron, effectively decreasing the barrier height and  $\beta$ . Many observed  $\beta$  values are available from DBA<sup>5,11,80,81</sup> and electrochemical experiments,<sup>16,20,82,83</sup> and they vary from  $\sim 1.0 \text{\AA}^{-1}$  for linear alkanes down to less than  $0.1 \text{\AA}^{-1}$  for certain conjugated bridges. ET is still coherent, meaning that the electron does not dephase during tunneling, and should not be viewed as “residing” on the gap molecule.

As the gap width increases beyond  $\sim 15 \text{\AA}$ , coherent tunneling effectively stops, and transport must occur by a series of steps (Fig. 2C). Many treatments of transport between “sites” in a thin film have appeared under various names depending in part on the nature of the “sites”. Poole–Frenkel transmission between coulombic “traps” refers to motion of electrons between potential wells in a solid, such as defects in a crystal.<sup>73,84</sup> “Redox exchange” refers to ET between redox centers in a redox polymer, often accompanied by ion motion.<sup>85–89</sup> “Hopping” is a term often used to describe redox exchange in conducting polymers, in which the “sites” may be small conducting domains known as polarons.<sup>23,90–92</sup> “Diffusive” or “incoherent” tunneling refers to a sequence of steps between possibly shallow potential wells.<sup>75,77</sup>

Redox exchange deserves special note because it represents an extreme opposite to that of coherent tunneling. The latter process requires no motion of nuclei, is virtually instantaneous, and is independent of temperature. In contrast, redox exchange is thermally activated and governed by a rate constant related to a free energy change *via* Marcus theory.<sup>23,85,88,93–97</sup> Once a “site” is occupied by an electron, there is nuclear reorganization of the associated molecular structure to result in a discrete charge center. The associated reorganization energy is reflected in the exponential temperature dependence of ET by redox exchange, and the existence of

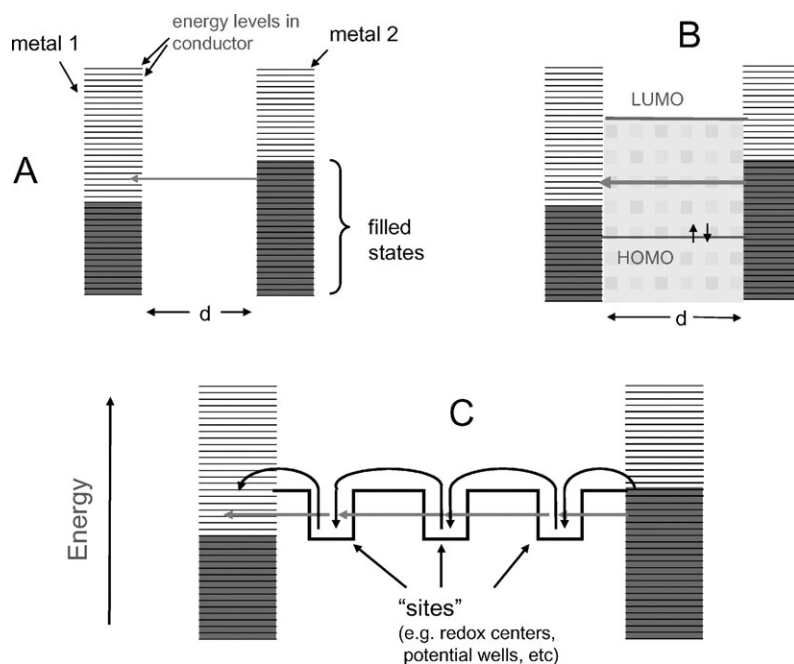


**Fig. 2** A. Energy levels for a vacuum gap between two conductors, with the shaded regions in the conductors representing filled electronic states, and the arrow representing coherent electron tunneling. B. Tunneling through a molecular layer between two conductors spaced apart by a distance  $d$ . C. “Incoherent” or “diffusive” tunneling (straight arrows) and activated redox exchange (curved arrows) among “sites” or redox centers in a relatively thick molecular layer.

multiple steps permits ET across distances much greater than those possible for coherent tunneling. To reiterate, coherent tunneling is short-range, very fast, and weakly temperature dependent, while redox exchange is slower, long range and thermally activated. In Fig. 2C, the straight grey arrows represent diffusive tunneling, while the black arrows denote an activated process such as redox exchange, with accompanying nuclear motion.

Table 1 also includes Schottky (*i.e.* thermionic) and field emission, which are normally associated with interfaces rather than “bulk” materials. Both are strongly dependent on the presence of an electric field but have very different dependences on temperature. It should be noted that electric fields present in molecular junctions may be very high across the nanoscale dimension, often exceeding  $10^6$  V cm<sup>-1</sup>, so that relatively uncommon conduction mechanisms such as field emission may become effective.

## 2. Fabrication of carbon-based molecular junctions

Our approach to junction fabrication differs from the more common Au/thiol self assembled monolayer (SAM) and Langmuir–Blodgett (LB) structures, mainly in the nature of the molecule/substrate bond. LB<sup>61,98–101</sup> and SAM<sup>102–106</sup> structures are essentially two-dimensional crystals which result as equilibrium configurations resulting from dynamic interactions between the molecules and a substrate. Although the Au–S bond in SAMs forms quickly, the monolayer then anneals slowly by repeated breaking and making of the Au–S bond until a stable, ordered array results as the minimum energy conformation. Similarly, LB films are “packed” by the Langmuir trough until an ordered array is indicated by changes in surface tension. Both SAM and LB structures can have excellent ordering over several microns of monolayer surface, but this ordering comes with the price of a relatively

**Table 1** Conduction mechanisms in metal/molecule/metal thin film junctions<sup>a</sup>

	Temperature ( $T$ ) dependence	Voltage ( $V$ ) dependence	Monolayer thickness ( $d$ ) dependence
Coherent tunneling, “superexchange”	None	linear (low $V$ ) exponential (high $V$ )	$\exp(-\beta d)$
Incoherent, diffusive tunneling	None (see text)	linear (low $V$ ) exponential (high $V$ )	$\exp(-cd)$
“Hopping,” including redox exchange	$\exp(-a/T)$	linear (low $V$ )	$d^{-1}$
Band transport	Weak	linear	$d^{-1}$
Poole–Frenkel effect (“traps”)	$\exp(-a/T)$	$\exp(bV^{1/2})$	$\exp(-cd^{1/2})$
Thermionic (Schottky) emission	$\exp(-a/T)$	$\exp(bV^{1/2})$	$\exp(-cd^{1/2})$
Field emission (“Fowler–Nordheim”)	None	$V^2 \exp(-b/V)$	$\exp(-cd)$

<sup>a</sup> The  $a$ ,  $b$ , and  $c$  denote constants which are independent of temperature, voltage, and thickness, respectively. Adapted from a similar table presented by Sze,<sup>84</sup> with additions from references cited in the main text.

weak molecule/substrate bond, ranging from  $<0.5$  eV for LB structures to  $\sim 1.6$  eV for the Au–S bond. Without the relatively weak surface bond, the LB and SAM monolayers would not be able to anneal to achieve long-range order.

A less common surface bonding mode involves a much stronger bond between the adsorbed molecule and a silicon or silicon oxide substrate.<sup>107–116</sup> The 3–4 eV bond energies of Si–C and Si–O–C bonds should result in substantially more stable devices, although applications in molecular junctions are currently limited. In one report, the Si–O–C bond appeared to be more stable than the Si–C bond with respect to reactions with vapor deposited metals.<sup>112</sup>

## 2.1 Carbon–carbon bond formation by aryl diazonium ion reduction

A fundamental distinction of carbon-based molecular junctions compared to SAM and LB approaches is irreversible formation of a covalent C–C bond by diazonium ion reduction, shown in Fig. 3. Surface bonding to metals, silicon, carbon fibers, diamond, and glassy carbon by diazonium reduction has been studied extensively,<sup>117–128</sup> but the current discussion will be limited to pyrolyzed photoresist film (PPF) substrates,<sup>129,130</sup> discussed in more detail below. Alternative methods for bonding to glassy carbon and diamond have been investigated by Hamers, *et al.*<sup>131–133</sup> and characterized in solution by electrochemistry.<sup>134</sup> While these approaches lead to strong carbon–carbon bonds and stable surfaces, they have not yet been employed in molecular junctions.

Three important features of covalent bonding to PPF *via* diazonium reduction motivated our incorporation of the reaction into the fabrication of molecular junctions. First, the C–C bond is strong ( $\sim 4$  eV, or  $100$  kcal mol<sup>-1</sup>) and is formed irreversibly, resulting in a surface modification stable to  $> 500$  °C. One would not expect surface reconstruction or detachment with such a strong surface bond. Second, the most likely bonding geometry is between the phenyl radical formed by diazonium reduction and a graphitic edge site of the PPF.<sup>135</sup> Although the precise bonding geometry resulting from diazonium reduction on disordered graphite has not been established, radical attack at the graphitic basal plane is much slower than at edge sites.<sup>136</sup> In fact, the reduction of diazonium reagents on graphite basal plane surfaces results in nucleation at edge plane defects to form multilayer “mushrooms” before attack of the basal plane.<sup>136,137</sup> In the case of

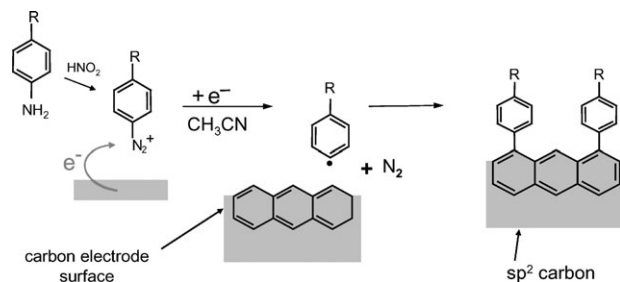


**Fig. 3** Covalent bonding of aromatic molecules to a graphitic carbon surface *via* reduction of aryl diazonium reagents. Phenyl radicals can bond to an unsatisfied surface valence or across a double bond.

carbon nanotubes, extensive reaction with diazonium reagents leads to changes in the electronic properties of the nanotube, presumably due to disruption of aromaticity by reactions at basal “wall” sites.<sup>138,139</sup> Since PPF has a high density of edge sites, radical addition is kinetically strongly favored at edge sites, presumably through addition to a double bond or coupling with an unsatisfied valence. The most likely result in either case is a phenyl–phenyl bond between the monolayer and the extended graphitic  $\pi$  system. The symmetry and low dipole moment across such a bond should result in a low barrier for electron injection from the PPF to the molecule. Third, since the phenyl radical is generated by an electron from the substrate, the process “actively” fills pinholes. Radical formation is fastest at exposed PPF, exactly where radicals are needed to completely cover the substrate surface. In fact, diazonium reduction can be “too aggressive” in that radical generation by tunneling or conduction through the initial monolayer can result in multilayers up to  $\sim 20$  nm thick.<sup>125,137</sup> It is standard practice in our laboratory to verify the thickness of molecular layers formed by diazonium reduction with AFM, as described below. The diazonium tetrafluoroborate reagents used to make the junctions described in this report were made from the corresponding amine precursors of biphenyl (BP), fluorene (FL), nitrobiphenyl (NBP) and nitroazobenzene (NAB). To reiterate the properties of diazonium reduction as a means of carbon surface modification: it results in strong C–C bonds and a very low pinhole density, but the monolayer is not as ordered as a SAM and is prone to multilayer formation. The exact nature and geometry of the C–C surface bond is a topic of current investigation, but it is likely to maintain conjugation between the graphitic  $\pi$  system and the phenyl ring of the modification layer. Molecular layers bonded to carbon surfaces by diazonium reduction have been characterized by XPS, AFM, Raman and IR spectroscopy, SIMS, and STM.<sup>118,124,125,135,137,140</sup> Several examples of spectroscopic characterization are given below for the case of PPF as the substrate.

## 2.2 Pyrolyzed photoresist film (PPF) substrate

The substrate for a molecular junction must be flat, on a length scale which is short compared to the monolayer thickness, to reduce the possibility of direct contact between the substrate and top conductor. As noted above, the atomically flat basal plane of graphite is not suitable for diazonium modification because the radical attaches first to defects which then become nuclei for forming “mushrooms”. Graphite edge plane is ideal from the reactivity standpoint, but no one has successfully prepared an edge plane surface which is flat on a molecular scale. An unusual form of graphitic carbon which is sufficiently flat and also permits modification by diazonium ions is essentially a form of glassy carbon.<sup>130,141–143</sup> A commercial photoresist is often based on a Novolac phenolic resin (AZ P4330-RS, AZ Electronic Materials USA Corp., Somerville, NJ), which is designed to adhere well to silicon and SiO<sub>2</sub>. After spin coating onto Si with a  $\sim 200$  nm oxide layer or quartz, the photoresist may be patterned with conventional soft-UV lithography if desired, as shown in Fig. 4. The Raman spectrum and conductivity of PPF depend on heat treatment

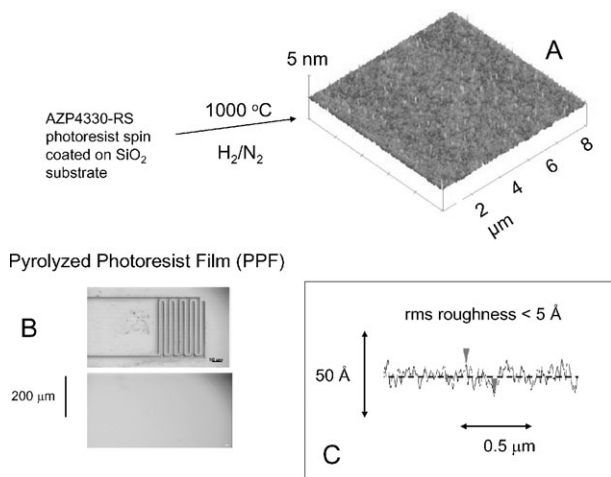


**Fig. 4** PPF formed by pyrolysis of photoresist resin in a hydrogen atmosphere. A. AFM image of PPF following pyrolysis; B. micrographs of patterned and unpatterned PPF samples on silicon; C. AFM line profile of PPF showing rms roughness of  $< 5 \text{ \AA}$ .

temperature, and approach those of glassy carbon for temperatures above  $1000 \text{ }^\circ\text{C}$ .<sup>129</sup> The PPF used for molecular junctions has a resistivity of  $0.006 \text{ } \Omega \text{ cm}$ , compared to  $0.0055 \text{ } \Omega \text{ cm}$  for glassy carbon heat treated at  $2000 \text{ }^\circ\text{C}$ . TEM and Raman spectroscopy indicate randomly oriented graphitic crystallites with sizes less than  $\sim 5 \text{ nm}$ .<sup>129</sup> The line scan in Fig. 4 indicates that PPF has an rms surface roughness of  $< 0.5 \text{ nm}$ .<sup>130</sup>

Single crystal graphite is a semimetal with a small overlap ( $\sim 0.06 \text{ eV}$ ) of the valence and conduction bands at the Fermi level.<sup>144</sup> However, disorder increases the electronic density of states (DOS) near the Fermi level to result in a DOS which does not vary greatly with energy. Although carbon materials sometimes exhibit n-type behavior for heat treatments below  $700 \text{ }^\circ\text{C}$ , the  $1000 \text{ }^\circ\text{C}$  treatment results in no observable n- or p-type behavior in PPF. Single crystal graphite is a very anisotropic conductor, with conductivity parallel to the graphite planes exceeding that perpendicular to the planes by a factor of  $\sim 1000$ .<sup>145</sup> However, PPF, like other disordered graphitic materials, is isotropic in electrical conductivity, heat transfer, *etc.* Electronically, PPF acts as a metal with con-

ductivity approximately 0.1% that of gold, and no observable band gaps. Unlike a metal, however, PPF can participate in surface bonding reactions which result in a strong carbon-carbon bond, a property vital to the current application.

### 2.3 Molecule/PPF characterization

The bonding and orientation of organic molecules bonded to PPF *via* aryldiazonium reduction was examined with Raman and FTIR spectroscopy and AFM.<sup>69,125,146,147</sup> Nitrozoabenzene (NAB) was prominent in early investigations because of its strong, preresonant Raman scattering of  $514.5 \text{ nm}$  light. As noted earlier, NAB phenyl radicals formed by electrochemical reduction of the  $\text{NAB-N}_2^+$  bond primarily to edge plane sites on the PPF surface. Previous experiments on NAB bonded to the edge plane of highly ordered pyrolytic graphite (HOPG) indicated that the NAB phenyl group adjacent to the surface was rotationally disordered relative to the edge plane, but also that the NAB scattering was unexpectedly strong.<sup>135</sup> The electronic interaction between the NAB and graphitic  $\pi$  system apparently shifted the NAB resonance Raman profile closer to the  $514.5 \text{ nm}$  laser, thus increasing the scattering intensity compared to NAB in solution by a factor of  $> 100$ .

An AFM line profile of PPF following NAB modification is shown in Fig. 5. In a study of mono- and multilayer formation with AFM, we reported that the rms roughness increased from  $0.155 \text{ nm}$  for bare PPF to  $0.236$ ,  $0.504$ , and  $0.143 \text{ nm}$  for BP, NBP, and NAB monolayers, respectively.<sup>125</sup> Fig. 5 also shows a non-contact image and line profile through a “trench” made with contact mode AFM using a force sufficient to remove the molecular layer but not sufficient to damage the much harder PPF (as judged by control experiments on unmodified PPF). Using a statistical procedure based on many line profiles at different positions across the “trench”, the thickness of the molecular layer could be determined with a precision of  $1\text{--}3 \text{ \AA}$ .

Both Raman spectroscopy of NAB and AB monolayers and IR spectroscopy of NAB, BP, NBP, and FL layers bonded to PPF *via* diazonium reduction indicate that the long axis of the molecules is oriented approximately parallel to the surface normal.<sup>147</sup> The relative intensities of Raman scattering for *s*- and *p*-polarized light are dramatically different for chemisorbed and physisorbed molecules, as are the IR absorbances

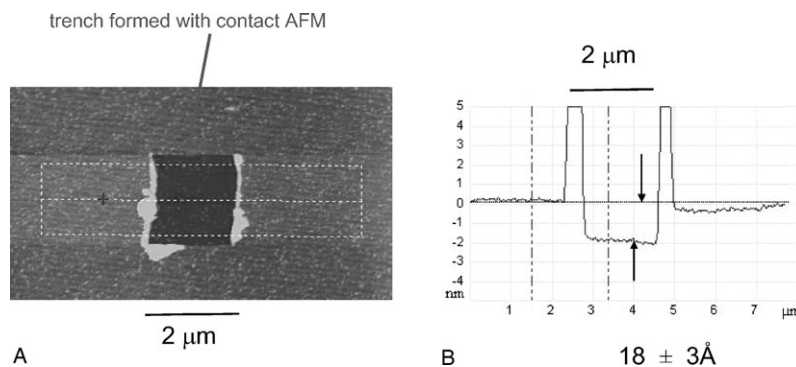


**Fig. 5** A. Image of a “trench” cut into a fluorene layer bonded to PPF using contact mode AFM, but imaged in non-contact mode. B. Line profile obtained with non-contact AFM through the trench. Statistical analysis of several lines covering most of the trench yielded an average depth of  $18 \pm 3 \text{ \AA}$ , the detailed procedure is given in ref. 125.

of in-plane to out-of-plane vibrations. Chemisorbed NAB and FL have average tilt angles relative to the surface normal of 31 and 44°, respectively, while the physisorbed molecules are nearly flat on the PPF surface. Furthermore, both Raman and infrared spectra of chemisorbed molecules are similar to the free molecules in a KBr pellet (except for relative intensities), indicating that the expected structures are maintained upon chemisorption. As noted above, the diazonium route does not yield an ordered 2-dimensional crystal, but the chemisorbed molecules are largely perpendicular to the surface with a layer thickness constant to  $<5 \text{ \AA}$  rms.

#### 2.4 Metal top contact deposition

Deposition of a metal contact on top of the molecular layer without penetration of the metal to form “shorts” has proven to be a challenge. SAMs often restructure and even reorient on top of a vapor deposited metal atom after it penetrates the initial monolayer.<sup>148–152</sup> A reactive end group on the SAM has been shown to “trap” metal atoms on the surface, as desired for making a molecular junction, although metals such as Ti appear to damage the molecular layer.<sup>151–153</sup> The strong C–C bond formed by diazonium reduction on PPF is an asset during metal deposition, since it cannot restructure and is more tolerant of the temperature increases expected from the heat of condensation of gas phase metal atoms. The 200–500  $\text{kJ mol}^{-1}$  (2–5  $\text{eV atom}^{-1}$ ) energy released upon metal condensation can lead to significant heating of the monolayer, even if the gaseous atom’s incident kinetic energy is negligible.

We initially used a Hg drop as the top contact,<sup>64–66</sup> as have other laboratories studying SAM junctions.<sup>38,154–157</sup> Uncertainty about junction area and likely impurities on the Hg or monolayer surface led us to consider electron beam evaporation. Several early reports on molecular junctions used titanium deposited by e-beam evaporation,<sup>39,60,62,158</sup> and alternatives like Au and Cu had been shown to penetrate SAMs and yield numerous short circuits. By operating the e-beam near threshold for atom emission and a pressure of  $\sim 10^{-6}$  Torr, we generated Ti atoms with low kinetic energy ( $<0.01 \text{ eV}$ ), and we used slow deposition rates for the initial layers of Ti atoms ( $\sim 0.03 \text{ nm s}^{-1}$ ).<sup>67,159</sup> The metals were deposited through a shadow mask to make junctions of two configurations: “spot” and “crossed”. Spots were made on a homogeneous surface of PPF modified with the relevant molecule, through a 0.50 mm diameter hole in aluminium sheet metal, to yield a junction area of  $0.0020 \text{ cm}^2$ . The top metal was then contacted lightly with a loop of Pt wire and a micromanipulator. Repeated contact of a given spot fourteen times yielded a relative standard deviation of junction resistance of 13%, indicating minimal damage during repeated contact. Electronic response of the junction was observed by application of a bias between the circular top contact and a probe positioned on the face of the PPF near the spot.

The crossed junction design was developed after the spot, and is more attractive in terms of smaller area and minimal concern about device damage by probes.<sup>69,71,147</sup> Photolithography with positive photoresist on  $\text{SiO}_2$  or  $\text{Si}_3\text{N}_4$  on Si produced PPF lines 0.5–1.0 mm wide and a few  $\mu\text{m}$  thick. After pyrolysis, the PPF was modified by diazonium reduc-

tion, then metal was deposited through a shadow mask with 0.1–0.5 mm wide stripes oriented perpendicular to the PPF lines. A photo of the finished junction is shown in Fig. 6, with pertinent features labeled. The current/voltage response of crossed junctions was obtained in either “3-wire” or “4-wire” geometry, in order to compensate for resistance in the PPF, metal film, and probe contacts. Probes for a 3-wire configuration are visible in Fig. 6, with the bias applied between  $V_{\text{drive}}^+$  and  $V_{\text{drive}}^-$ . The probe labeled “ $V_{\text{sense}}^+$ ” was used in a 3-wire configuration to correct for the substantial resistance ( $10^2$ – $10^3 \Omega$ ) in the PPF “wire” and associated contact. The resistance of the metal “wire” was significantly lower (generally  $<20 \Omega$ ), but could be corrected with a fourth wire on the opposite end of the metal lead if necessary ( $V_{\text{sense}}^-$ ). Unless noted otherwise, electronic characterization was carried out at room temperature in air, with a 3-wire arrangement.

#### 2.5 Metal oxide deposition

As will be described below, the oxidation states of both the molecular layer and the metal play a critical role in junction electronic behavior. At typical deposition pressures ( $10^{-7}$ – $10^{-6}$  Torr), Ti is easily oxidized by residual  $\text{H}_2\text{O}$  and  $\text{O}_2$ , to produce  $\text{Ti}^{\text{II}}$ ,  $\text{Ti}^{\text{III}}$  and  $\text{Ti}^{\text{IV}}$  oxides in addition to Ti metal.<sup>71,159–161</sup> Furthermore, Ti and most metal atoms are reducing agents which can reduce NAB and related molecules. We used Raman spectroscopy and XPS to examine NAB modified PPF following deposition of thin films (nominally 10–30  $\text{\AA}$ ) of Ti, Cu, and Au.<sup>146,162,163</sup> Fig. 7 shows Raman spectra of NAB on PPF before and after deposition of Ti or Cu with a nominal thickness (determined with a quartz crystal microbalance) of 10  $\text{\AA}$ . The decrease of the nitro stretch at  $\sim 1340 \text{ cm}^{-1}$  and the increase in the 1401/1450 peak intensity ratio indicates that the NAB is partially reduced upon metal deposition.<sup>164</sup> Furthermore, XPS shows formation of a Ti–N bond following Ti deposition and a Cu–N bond following Cu deposition. Although the  $1340 \text{ cm}^{-1}$  band intensity is not a direct quantitative measure of NAB reduction, it provides a semiquantitative indication. Table 2 shows the 1340/1142

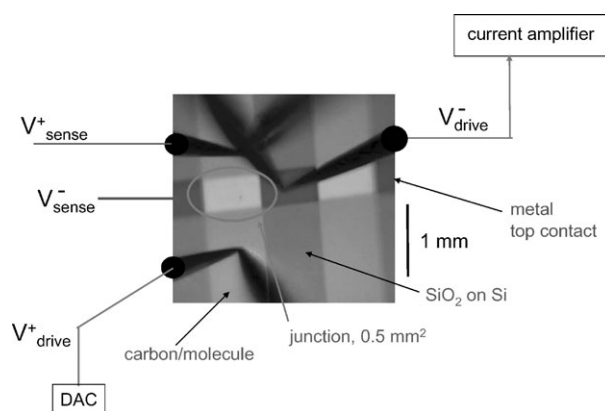


**Fig. 6** Video photograph of a finished  $\text{Si/SiO}_2/\text{PPF/NAB}(4.5)/\text{AlO}_x(3.0)/\text{Au}$  junction. Bias is imposed between  $V_{\text{drive}}^+$  and  $V_{\text{drive}}^-$ , and current amplifier input is held at virtual ground.  $V_{\text{sense}}^+$  is a high impedance input which can be used to correct the applied bias for ohmic losses in the PPF;  $V_{\text{sense}}^-$  may be used similarly to correct for metal lead resistance.

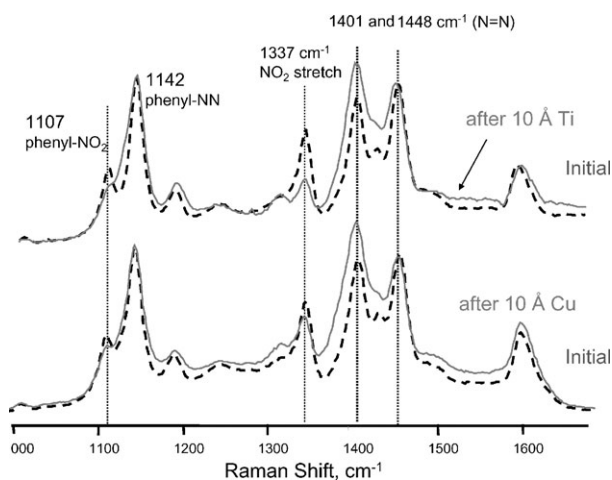


**Fig. 7** Surface Raman spectra obtained with a 514.5 nm laser before and after deposition of a nominal thickness of 10 Å of Ti (upper pair) or 10 Å of Cu (lower pair). Dashed curves were acquired before metal deposition; solid curves after. Each pair was normalized to have equal intensities of the 1142 cm<sup>-1</sup> band. Adapted in part from ref. 163.

cm<sup>-1</sup> ratio for several metals on NAB, as well as the presence of a metal–nitrogen bond indicated by XPS of NAB films following deposition of 10 Å of metal. It should be noted that the Raman spectrum of the NAB is largely unaltered as a consequence of metal deposition, indicating that the surface molecules are intact. Some attenuation of the entire spectrum was observed, due to absorption losses of laser and scattered light in the metal film.

Various combinations of modified PPF and top metals were prepared with large areas (~2 cm<sup>2</sup>) but with the same deposition conditions and thicknesses used to make junctions for electronic characterization. Following deposition, the samples

were transferred in air to an XPS equipped with an Ar<sup>+</sup> ion beam for depth profiling. The simplest case was PPF/biphenyl/Cu in which the molecule contains no oxygen and Cu is a relatively noble metal which should be less reactive with residual gases. Ar<sup>+</sup> sputtering through the Cu and biphenyl layers and into the PPF revealed no detectable oxygen, confirming that both Cu deposition and exposure to air did not introduce oxides into the junction interior.<sup>71,163</sup> In contrast, Al deposited at 4 × 10<sup>-6</sup> Torr is completely Al<sup>III</sup> with no detectable Al<sup>0</sup> by XPS.<sup>71,162</sup> The oxygen is present mostly as hydroxide, as might be expected if the residual gas is primarily H<sub>2</sub>O rather than O<sub>2</sub>. As noted in Table 2, Al, Cu and Ti show evidence of metal–N bond formation when the metals are deposited on NAB monolayers.

Ti cannot be deposited as pure Ti<sup>0</sup> without UHV conditions, and typical e-beam pressures of 10<sup>-8</sup>–10<sup>-6</sup> Torr yield a range of Ti oxides. Furthermore, extended exposure to air slowly increases the Ti oxidation state, with significant effects on electronic behavior (see below). XPS depth profiling of PPF/NAB/TiO<sub>x</sub> (3.0)/Au junctions with a backpressure during Ti deposition of 2.8 × 10<sup>-7</sup> Torr showed Ti<sup>0</sup>, Ti<sup>II</sup>, and Ti<sup>III</sup> in the junction with oxygen present as an oxyhydroxide.<sup>71,160,163</sup> After 1 year in ambient air, the Ti<sup>IV</sup> content increased from <5% to ~50%. Intentional exposure of the deposited Ti to air before being protected with Au resulted in junctions without detectable Ti<sup>0</sup>, Ti<sup>II</sup> or Ti<sup>III</sup>, but with higher conductance than expected for pure TiO<sub>2</sub>.<sup>71</sup> As will be discussed later, further oxidation by depositing TiO<sub>2</sub> from rutile in the presence of O<sub>2</sub> had significant electronic effects.

Once we became aware of the important role of metal oxides in junction behavior, we pursued three junction types: (1) PPF/molecule/Cu/Au junctions with negligible oxide present, (2) PPF/molecule/AlO<sub>x</sub>/Au junctions with intentionally oxidized Al, and (3) PPF/molecule/TiO<sub>x</sub>/Au junctions containing

**Table 2** Raman and XPS results for nitroazobenzene multilayers (3.7–4.5 nm) following metal deposition<sup>162,163</sup>

Metal/nm <sup>a</sup>	N <sup>b</sup>	1340/1142 cm <sup>-1</sup> intensity ratio	S.D. <sup>c</sup>	1400/1450 intensity ratio	S.D. <sup>c</sup>	Metal–N bond in XPS?
None	5	0.733	0.03	0.976	0.01	
Au(1) <sup>d</sup>	3	0.668	0.01	0.994	0.004	Undetected
Au(10)	6	0.668	0.01	1.11	0.011	
Au(10) after 18 days	6	0.685	0.02	1.097	0.012	
Ag(1)/Au(9) <sup>e</sup>	6	0.655	0.02	1.203	0.02	Weak, 398.0 eV
Ag(3)/Au(7)	9	0.433	0.01	1.304	0.018	
Ag(3)/Au(7) after 60 days	9	0.475	0.02	1.159	0.014	
Cu(1) <sup>e</sup>	4	0.61	0.03	1.223	0.056	Yes, 398.4
Cu(3)/Au(7)	3	0.426	0.03	1.694	0.01	
Cu(3)/Au(7) after 60 days	3	0.504	0.02	1.292	0.092	
Ti(1)/Au(9) <sup>d</sup>	3	0.348	0.03	1.499	0.085	Yes, 397.0
Ti(3)/Au(7) <sup>d</sup>	3	0.444	0.02	1.629	0.041	
Ti(1)/Au(90) after 14 days	3	0.427	0.02	1.194	0.114	
Al(1)/Au(9) <sup>e</sup>	6	0.477	0.03	1.07	0.035	Undetected
Al(3)/Au(7) <sup>e</sup>	6	0.244	0.03	1.732	0.084	
Al(3)/Au(7) after 30 days	6	0.246	0.03	1.446	0.081	

<sup>a</sup> Samples less than 24 h old unless noted otherwise. <sup>b</sup> Number of samples. <sup>c</sup> Standard deviation of peak intensity ratio. <sup>d</sup> Metal deposited at (4–8) × 10<sup>-6</sup> Torr. <sup>e</sup> Metal deposited at <5 × 10<sup>-7</sup> Torr.

varying amounts of  $\text{Ti}^{\text{IV}}$ . The first two types represent junctions with either conducting or insulating top contacts, and the Ti junctions have a range of properties between these two extremes. Unless noted otherwise, electronic characterization was done within one day of metal deposition in air at ambient temperature. Junction designations below include the layer thickness in nanometers determined from AFM, *e.g.* NAB (4.5) indicates an NAB film thickness of 4.5 nm. All current/voltage characteristics are presented as current density *vs.* voltage ( $J/V$ ) curves, with the voltage polarity as PPF relative to the protective Au on the top metal or metal oxide contact. Positive current corresponds to electron transport through the junction from the Au to PPF.

### 3. Electronic behavior of PPF/molecule/Cu/Au junctions

Results for molecular junctions made with a Cu top contact and three different molecules are shown in Fig. 8, and the junction resistances observed at low bias are summarized in Table 3. While molecular structure has strong effects on the observed current density *vs.* voltage curves ( $J/V$  curves), the Cu junctions have several characteristics in common.<sup>70</sup> First, the  $J/V$  curves are very nonlinear, with weak or negligible rectification. Second, the curves are invariant with scan rate over a range of 1–1000  $\text{V s}^{-1}$ , and exhibit no observable hysteresis. Third, all junctions types represented in Fig. 8 were unchanged after thousands of voltage cycles, with several tested to  $>10^8$  cycles. Fourth, Cu junctions showed only minor increases in resistance with time, by a factor of  $\sim 2$  over a month of exposure to air. Fifth, the yield of working junctions was 96%, with three of a total of 72 junctions rejected due to non-repeatable  $J/V$  curves.<sup>70</sup> The relative

standard deviations of the resistance of a given junction type were typically 5–15%. Finally, the Cu junctions showed a weak temperature dependence, with increased resistance at lower temperatures. Over a limited range of 214–310 K, plots of  $\ln G$  *vs.*  $1/T$  were linear with slopes of 0.064, 0.075 and 0.083 eV for BP, FL, and NBP, respectively, where  $G$  is the conductance in the bias range of  $\pm 50$  mV.

The dependence of the  $J/V$  response on molecular structure is important since it indicates that junction conductance is affected significantly by molecular properties rather than some experimental artifact. A particularly convincing comparison is between biphenyl and fluorene junctions, which have the same PPF/molecule and molecule/Cu interfaces, the same thickness and nearly the same molecular structure. However, the planar fluorene molecule yields junctions with  $\sim 11$  times the conductance of those of biphenyl, which is expected to have a  $\sim 36^\circ$  dihedral angle between its phenyl rings based on the free molecule. NBP junctions are  $\sim 35$  times as conductive as BP junctions, presumably due to the Cu–N covalent contact expected from the XPS results listed in Table 2. Extensive theoretical and experimental investigations of metal/molecule/metal junctions has shown that the conductance is a function of the entire electronic system, including the nature of the contacts and the conformation of the molecules in the finished junction.<sup>36,37,39,40,56,61,63,74,97,165–171</sup> Although the detailed effects of junction structure on transport are likely to be complex, the results illustrated in Fig. 8 indicate that molecular structure is a significant factor, and that the barriers associated with the PPF–molecule and metal–molecule “contacts” do not completely dominate junction conductance.<sup>70</sup>

Fig. 8C is a plot of  $\ln(J)$  *vs.*  $V$  over three orders of magnitude of current density for monolayer/Cu junctions.  $J$  is approximately linear with  $V$  at low bias, then becomes exponential with

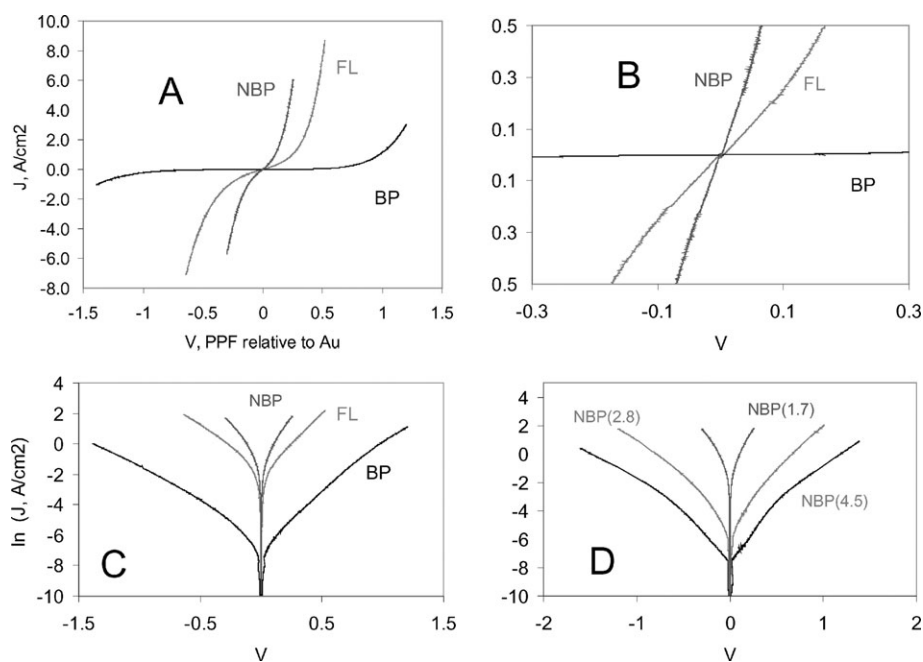


**Fig. 8** Current density/voltage curves for PPF/molecule/Cu/Au junctions obtained at room temperature and 100  $\text{V s}^{-1}$  (A, B). Note scale expansion in panel B. C and D are similar curves plotted as  $\ln(J)$  *vs.*  $V$ , obtained at a range of scan rates (0.1–10  $\text{V s}^{-1}$ ) to cover a wide sensitivity range.

**Table 3** Observed junction resistances for PPF/molecule/metal oxide/metal molecular junctions

Junction	Molecule (thickness/nm) <sup>a</sup>	Oxide (if present) (thickness/nm)	Top contact (thickness/nm)	Resistance <sup>b</sup> /Ω cm <sup>2</sup> , $V = \pm 50$ mV 10 V s <sup>-1</sup>	Resistance rsd <sup>c</sup> (%)	Ref.
PPF/Cu	None	None	Cu(30)/Au(10)	0.0041	1.1	70
PPF/BP/Cu	Biphenyl (1.6)	None	Cu(30)/Au(10)	4.46	2.6	70
PPF/FL/Cu	Fluorene(1.7)	None	Cu(30)/Au(10)	0.40	8.5	70
PPF/NBP/Cu	Nitrobiphenyl (1.7)	None	Cu(30)/Au(10)	0.13	21	70
PPF/NBP/Cu	Nitrobiphenyl (2.8)	None	Cu(30)/Au(10)	11.5	1.4	70
PPF/NBP/Cu	Nitrobiphenyl (4.3)	None	Cu(30)/Au(10)	160.0	1.5	70
PPF/NAB/Cu	Nitroazobenzene(4.5)	None	Cu(3)/Au(7)	1.73	7.5	71
PPF/AlO <sub>x</sub>	None	AlO <sub>x</sub> (3.3)	Au(7)	1730	9.8	71
PPF/NAB/AlO <sub>x</sub> /Au	Nitroazobenzene(1.9)	AlO <sub>x</sub> (3.3)	Au(7)	2620	13	71
PPF/NAB/AlO <sub>x</sub> /Au	Nitroazobenzene(4.5)	AlO <sub>x</sub> (3.3)	Au(7)	9620	7.9	71
PPF/FL/AlO <sub>x</sub> /Au	Fluorene(1.7)	AlO <sub>x</sub> (3.3)	Au(7)	8970	5.5	71
PPF/TiO <sub>2</sub> /Au	None	TiO <sub>2</sub> from Ti (3.1) <sup>d</sup>	Au(7)	3.25		71
	None	TiO <sub>2</sub> from rutile(3.1) <sup>e</sup>	Au(7)	56	10	This work
	None	TiO <sub>2</sub> (O <sub>2</sub> ) <sup>ef</sup>	Au(7)	8600	68	This work
PPF/FL/TiO <sub>2</sub> /Au	FL(1.7)	TiO <sub>2</sub> from Ti (3.1) <sup>d</sup>	Au(7)	218	7.3	71
	FL(1.7)	TiO <sub>2</sub> from rutile(3.1) <sup>e</sup>	Au(7)	197	16	This work
	FL(1.7)	TiO <sub>2</sub> (O <sub>2</sub> ) <sup>ef</sup>	Au(7)	62 000	47	This work
PPF/NAB/Ti/Au	Nitroazobenzene(1.9)	None	Ti(3 <sup>g</sup> )/Au(7)	1.60	75	160
PPF/NAB/Ti/Au	Nitroazobenzene(4.5)	None	Ti(3 <sup>g</sup> )/Au(7)	6.10	48	160
PPF/NAB/TiO <sub>2</sub> /Au	NAB(1.9)	TiO <sub>2</sub> from Ti (3.1) <sup>d</sup>	Au(7)	56	29	71
	NAB(1.9)	TiO <sub>2</sub> from rutile(3.1) <sup>e</sup>	Au(7)	20	60	This work
	NAB(1.9)	TiO <sub>2</sub> (O <sub>2</sub> ) <sup>ef</sup>	Au(7)	41 000	28	This work
	NAB(4.5)	TiO <sub>2</sub> from Ti (3.1) <sup>d</sup>	Au(7)	370	5.4	71
	NAB(4.5)	TiO <sub>2</sub> from rutile(3.1) <sup>e</sup>	Au(7)	371	11	This work
	NAB(4.5)	TiO <sub>2</sub> (O <sub>2</sub> ) <sup>ef</sup>	Au(7)	50 200	85	This work

<sup>a</sup> Thickness determined with AFM on unmetallized samples. <sup>b</sup> Product of observed resistance and junction area in cm<sup>2</sup>. <sup>c</sup> Relative standard deviation (%) of junction resistance, for typically 4–8 junctions. <sup>d</sup> Ti deposited at  $\sim 8 \times 10^{-6}$  Torr, and exposed to air for 45 min before Au deposition. <sup>e</sup> Thickness based on deposition weight from quartz crystal microbalance, backpressure =  $8 \times 10^{-6}$  Torr. <sup>f</sup> From rutile with  $1 \times 10^{-5}$  Torr O<sub>2</sub> present. <sup>g</sup> Ti deposited at  $2.1 \times 10^{-7}$  Torr.

bias when  $|V| > 0.1$  V. In addition,  $\ln(J)$  decreases linearly with junction thickness for NBP multilayers over the range 1.6–4.6 nm, with a slope  $-0.22 \text{ \AA}^{-1}$  (Fig. 8D). Combined with the weak temperature dependence, the exponential voltage and thickness dependence are consistent with a tunneling mechanism for ET in PPF/molecule/Cu junctions (see Table 1). The observed resistances of NBP, FL, and BP junctions are in the same order as the HOMO–LUMO gaps (4.25, 5.04, 5.37 eV, respectively) of the free molecules calculated with density functional theory. It is too early to conclude that tunneling is the only ET mechanism, or that the tunneling is solely coherent or diffusive, but any ET mechanism proposed for PPF/molecule/Cu junctions must be consistent with weak temperature dependence and strong effects of molecular structure.

Based on several reports of SAM restructuring during metal deposition and the formation of metallic “short circuits” in metal/molecule/metal junctions,<sup>101,149–152,172</sup> it is reasonable to consider whether the  $J/V$  curves in Fig. 8 are actually due to metal filaments or other defects. Such “shorts” may represent a small fraction of the junction area, but may dominate junction conductance due to the high conductivity of metals compared to organic molecules. To attribute the large conductance variations apparent in Fig. 8 to defects, one would have to assume that NBP, FL, and BP had significantly different surface

coverages or packing arrangements, thus yielding a varying population of pinholes and filaments. However, the conclusion that pinholes or filaments have negligible effects on the  $J/V$  behavior is supported by some strong arguments.<sup>69,70</sup> Metallic conduction in filaments would not exhibit the nonlinear  $J/V$  curve of Fig. 8, and should have a  $d^{-1}$  dependence expected for ohmic behavior rather than the observed exponential thickness dependence. Conduction in metals should increase at lower temperatures, opposite to the observations. The twisted BP molecule should pack less well and leave more spaces for pinholes than planar FL molecules, yet BP junctions have the higher resistance. The possibility of filaments forming and breaking during voltage scans<sup>173</sup> is unlikely for the results of Fig. 8, since the observed curves are invariant with scan rate over three orders of magnitude. These arguments support the conclusion that the large variations in conductance apparent in Fig. 8 are due to molecular structure rather than some artifact of junction fabrication.

#### 4. Electronic behavior of PPF/molecule/AlO<sub>x</sub>/Au junctions

In the course of investigating the Ti/TiO<sub>x</sub> junctions introduced earlier, we made PPF/molecule/AlO<sub>x</sub>/Au junctions by

depositing Al at high backpressure ( $5 \times 10^{-6}$  Torr). XPS depth profiling showed the Al to be present as  $\text{Al}^{\text{III}}$  oxyhydroxide, presumably formed as a result of  $\text{Al}^0$  reacting with residual  $\text{H}_2\text{O}$  in the deposition chamber. Both  $\text{Al}_2\text{O}_3$  and  $\text{Al}(\text{OH})_3$  have a large HOMO–LUMO gap ( $>8$  eV) and are good insulators, which we investigated to provide a contrast to the semiconducting  $\text{TiO}_2$ .  $J/V$  curves for several PPF/molecule/ $\text{AlO}_x$  (3.0)/Au junctions are shown in Fig. 9. As expected, the conductance is much lower than the corresponding Cu junction (Fig. 9A), by  $\sim 4$  orders of magnitude for NAB(4.5).<sup>71,161</sup> There is some variation in  $J/V$  response with changes in molecular structure (Fig. 9C), but the  $J/V$  response is dominated by the insulating  $\text{AlO}_x$  layer. At  $|V| > 3$  V, the current density increases, presumably due to field emission across the  $\text{AlO}_x$  layer. Based on the Cu junctions, ET across the molecular layer is much faster than that across the  $\text{AlO}_x$ , hence the dominance of the  $J/V$  curve by the low  $\text{AlO}_x$  conductivity.

However, the model of an insulating  $\text{AlO}_x$  layer adjacent to a relatively conductive molecular layer is incomplete, given the results of *in situ* Raman spectroscopy of PPF/NAB(4.5)/ $\text{AlO}_x$ (3.0)/Au(7.0) junctions. The  $\text{AlO}_x$ /Au top contact is sufficiently transparent ( $\sim 50\%$ ) to permit observation Raman

scattering from a 514.5 nm laser to be collected while the junction is under bias.<sup>69,71</sup> Fig. 10A shows Raman spectra for a sequence of applied voltages, acquired in order from top to bottom. For the bias range of +1.0 to  $-1.5$  V (PPF relative to Au), there are reversible changes in the 1401/1450 intensity ratio, shown for three different junctions in Fig. 10B. As noted earlier, an increase of the 1401/1450 ratio correlates with reduction of the NAB to its quinoid anion.<sup>69,162,164</sup> For a bias negative of  $-1.5$  V, more dramatic spectral changes are observed, which indicate irreversible reduction of the nitro group. Spectral changes were also observed for azobenzene junctions which lacked the nitro group, with reversible loss of intensity of all bands for  $V = -3$  V.<sup>161</sup>

The spectroscopic results in Fig. 10 provide unequivocal evidence for structural changes within a PPF/NAB (4.5)/ $\text{AlO}_x$  (3.0)/Au junction, despite the fact that the  $J/V$  curve is essentially flat over the relevant voltage range. The Raman spectrum of the PPF/NAB (4.5)/ $\text{AlO}_x$ /Au junction biased at +1 V is similar to that of NAB chemisorbed to PPF without a metal overlayer, and represents the oxidized “phenyl” state. The increase in 1401/1450 ratio and decrease in nitro ( $1340\text{ cm}^{-1}$ ) intensity at  $-1.5$  V are similar to the spectral changes observed during electrochemical reduction of NAB to its reduced “quinoid” form. We reported in detail elsewhere the *in situ* Raman observation of electrochemical reduction of NAB bonded to glassy carbon and immersed in a non-aqueous electrolyte solution.<sup>164</sup> The reversible loss of Raman intensity at  $-3$  V is likely a result of a decrease of resonance enhancement in the “quinoid” NAB on PPF, due to a shift in the resonance Raman excitation profile. Furthermore, the spectrum at  $-2$  and  $-3$  V resembles that of dimethylaminoazobenzene, implying irreversible reduction of the nitro group.<sup>162</sup>

A relatively simple model which explains the observed structural changes is that of a very thin electrochemical cell with the  $\text{AlO}_x$  acting as an electrolyte separating two half reactions. For negative bias, NAB is reduced by electrons from the PPF, and an unknown cation from the  $\text{AlO}_x$  layer balances the resulting anionic  $\text{NAB}^-$ . In order to complete such a redox cell, there would need to be a corresponding oxidation at the Au electrode, either Au itself or some unknown oxidizable species such as residual  $\text{Al}^0$ . An alternative but more exotic model is the reduction of NAB driven by the high electric field in the junction. The  $\sim 3\text{ MV cm}^{-1}$  field present for a  $-2$  V bias across the  $\sim 8$  nm thick interior of the junction is comparable to the fields present in typical electrochemical double layers which bring about redox reactions at electrode surfaces in solution. If the reduction is field driven, the “counter ion” would be an image charge in the Au metal. In this model, there is no requirement for mobile charge or an oxidation to balance the NAB reduction.

It is both unexpected and interesting that spectral changes occur in an essentially solid state ultrathin layer device, whether or not it is a “complete” electrochemical cell with mobile electrolyte ions. However, the large barrier to electron transport from the  $\text{AlO}_x$  prevents these changes from significantly affecting the electronic properties of the junction. The analogous PPF/NAB/ $\text{TiO}_2$ /Au junctions have quite different electronic behavior, due to the much smaller band gap of  $\text{TiO}_2$  ( $\sim 3$  eV), as discussed next.

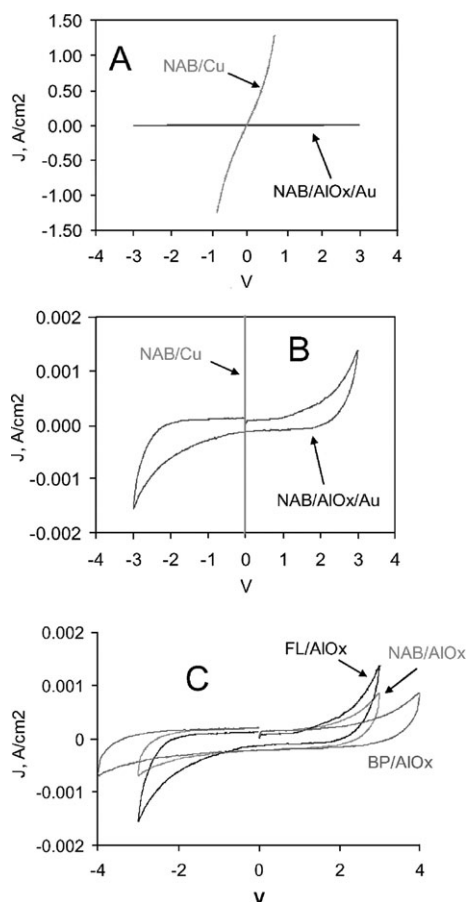


**Fig. 9** A.  $J/V$  curve for a PPF/NAB(4.5)/ $\text{AlO}_x$ (3.0)/Au junction compared to that for a PPF/NAB(4.5)/Cu(3.0)/Au junction, scan rate =  $100\text{ V s}^{-1}$ . B. Same data on a greatly expanded current density scale. C. Comparison of three different PPF/molecule/ $\text{AlO}_x$ (3.0)/Au junctions, all obtained at  $100\text{ V s}^{-1}$ .

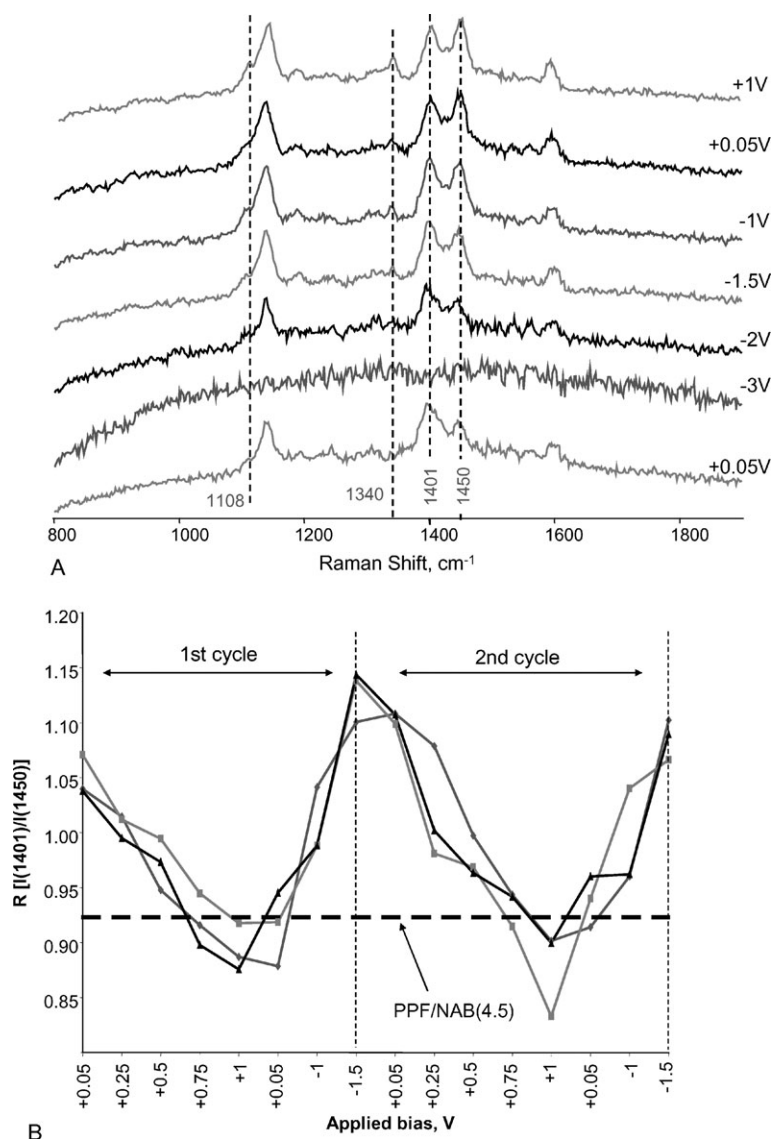


**Fig. 10** A. Raman spectra obtained for a PPF/NAB(4.5)/AlO<sub>x</sub>(3.0)/Au junction as a function of bias, all with a 514.5 nm laser. Sequence progressed from top to bottom, with the biases indicated. Acquisition time was 20 s after a given bias was imposed for 20 s, and a PPF spectrum was subtracted in all cases. B. Ratio of the 1401/1450 cm<sup>-1</sup> intensities for three independent PPF/NAB(4.5)/AlO<sub>x</sub>(3.0)/Au junctions during two bias excursions between +1 and -1.5 V. Adapted from ref. 71.

## 5. PPF/molecule/TiO<sub>x</sub>/Au junctions

The pronounced effects of Ti deposition conditions on electronic behavior of PPF/NAB(4.5)/TiO<sub>x</sub>(3.1)/Au molecular junctions are shown in Fig. 11 and summarized in Table 3. For the lowest deposition pressures achievable with our apparatus, PPF/NAB/Ti/Au junctions approach the high conductance observed with Cu and Au (Fig. 11A, Table 3). Although XPS indicates appreciable Ti<sup>II</sup> and Ti<sup>III</sup> oxyhydroxides in addition to Ti<sup>0</sup>, these oxides are essentially metallic, with conductivities within a factor of four of that of Ti metal. For example, over the thin dimension of Ti perpendicular to the PPF, Ti<sup>II</sup> oxide (resistivity = 170 μΩ cm<sup>174</sup>) should contribute much less than 1 Ω of resistance. The similarity of the *i/V* curves for Au, Cu, and Ti in Fig. 11A implies that the three metals deposited at ~3 × 10<sup>-7</sup> Torr are similar in terms of their electronic

interactions with NAB, despite their differences in work function.

### 5.1 Rectification in NAB/TiO<sub>2</sub> junctions

As the degree of oxidation increases for PPF/NAB/Ti/Au junctions, the *i/V* behavior changes dramatically, as shown in Fig. 11A and in 11B on an expanded current scale. The conductance at low voltage decreases by several orders of magnitude with a higher oxidation state of Ti (Table 3), and the junction becomes rectifying. If the Ti is intentionally oxidized to TiO<sub>2</sub> (as verified with XPS depth profiling), the junction is a rectifier and is stable for months.<sup>71</sup> However, even if the Ti in PPF/NAB(4.5)/TiO<sub>2</sub> junctions is intentionally oxidized, the TiO<sub>2</sub> junctions have significantly higher conductance than the corresponding AlO<sub>x</sub> junctions, all else being

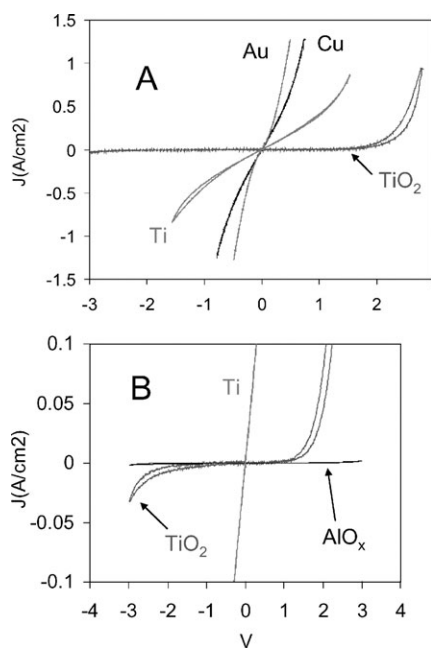


**Fig. 11** A.  $J/V$  curves ( $100 \text{ V s}^{-1}$ ) obtained for PPF/NAB(4.5)/metal/Au junctions for Cu, Au, and Ti top contacts, and varying oxidation state of the Ti. The curve labeled “TiO<sub>2</sub>” was obtained on a junction which was exposed to air between Ti and Au deposition. “Ti” was deposited from Ti metal at  $\sim 3 \times 10^{-7}$  Torr. All junctions had a final layer of Au. B. Comparison of NAB(4.5) junctions with the indicated top contacts, but on an expanded current density scale.

equal (Fig. 11B). Fig. 12A shows the effect of further oxidation of the TiO<sub>2</sub> deposit achieved by starting with rutile in the e-beam crucible instead of Ti, and also by backfilling the deposition chamber with O<sub>2</sub> to  $1 \times 10^{-5}$  Torr during TiO<sub>2</sub> deposition. The three cases shown in Fig. 12A are qualitatively similar with minor but reproducible quantitative differences, and all show significant rectification. The junctions have low conductivity unless the Au contact is biased negative relative to the PPF substrate (*e.g.*  $V > +2 \text{ V}$  in Fig. 12A), in which case electrons flow from the Au through the TiO<sub>2</sub> and NAB layers to the PPF.

Fig. 12B shows a “control” PPF/TiO<sub>2</sub>/Au junctions prepared with the same three deposition conditions as those for Fig. 12A. Comparing each pair of junction types, each with and without NAB, it is apparent that rectification occurs only with a NAB multilayer present. In addition, the hysteresis apparent in all the curves of Fig. 12A for positive bias also occurs for TiO<sub>2</sub> alone. The hysteresis is symmetric for the PPF/TiO<sub>2</sub>/Au junction, with the return scans from the positive and negative bias limits having larger current than the outgoing scans. The hysteresis for the PPF/NAB(4.5)/TiO<sub>2</sub>(3.0)/Au junctions is not symmetric, with the current magnitude decreasing during the negative going scan, rather than increasing. As will be shown below, this difference is mechanically important. It should also be noted that the addition of oxygen during TiO<sub>2</sub> deposition results in a significant decrease in the low voltage conductance for all junctions containing TiO<sub>2</sub> (Table 3). Presumably this decrease is caused by further reduction in the number of electrons available as charge carriers in the TiO<sub>2</sub> conduction band.

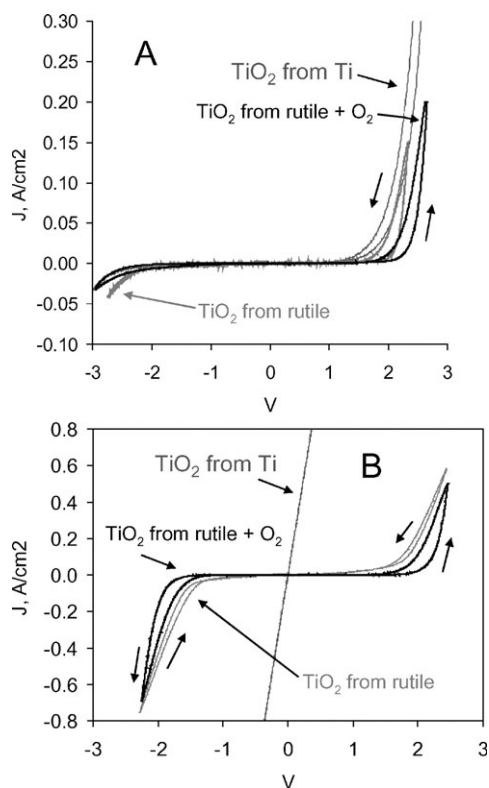


**Fig. 12** A.  $J/V$  curves for PPF/NAB(4.5)/TiO<sub>x</sub>/Au junctions prepared with different conditions of Ti oxide formation. Scans were initiated in a positive direction at  $100 \text{ V sec}^{-1}$ . Arrows indicate scan direction on various portions of the curves. B. PPF/TiO<sub>2</sub>/Au “control” junctions lacking an organic molecular layer but with otherwise identical conditions. Curves labeled “rutile” were for junctions made by e-beam deposition of TiO<sub>2</sub> from rutile, with or without  $1 \times 10^{-5}$  Torr of O<sub>2</sub> present during deposition, as indicated.

## 5.2 Raman spectroscopy of PPF/NAB/TiO<sub>x</sub>/Au junctions

*In situ* Raman spectra of PPF/NAB(4.5)/Ti(1.0)/Au junctions are shown in Fig. 13, as a function of bias. For zero bias, the 1401/1450 ratio of 1.06 indicates partial reduction of NAB during Ti deposition, since the junction of Fig. 13 was prepared by Ti deposition as metal rather than TiO<sub>2</sub>. As was the case with AlO<sub>x</sub> junctions (Fig. 10) positive bias causes a decrease in the 1401/1450 intensity ratio, and the ratio tracks applied bias for several cycles between  $-1$  and  $+3$  volts. Note that the 0.91 ratio observed at  $V = +3 \text{ V}$  persists after the bias is returned to zero, but returns to 1.06 at  $-1 \text{ V}$ , implying that the structural changes occurring at  $+3$  volts are at least metastable, consistent with hysteresis evident in the  $J/V$  curves.<sup>69</sup> As was the case with the AlO<sub>x</sub> junction, a bias negative of  $-1 \text{ V}$  causes partially irreversible spectral changes, although the spectrum did not completely vanish at  $-3 \text{ V}$ .

Structures for the oxidized and reduced forms of NAB are shown in Fig. 14. The “phenyl” and “quinoid” structures shown are examples of several resonance forms possible for their respective oxidized and reduced NAB species. These structures are those predicted from density functional theory for the native NAB and the singly reduced NAB anion, and

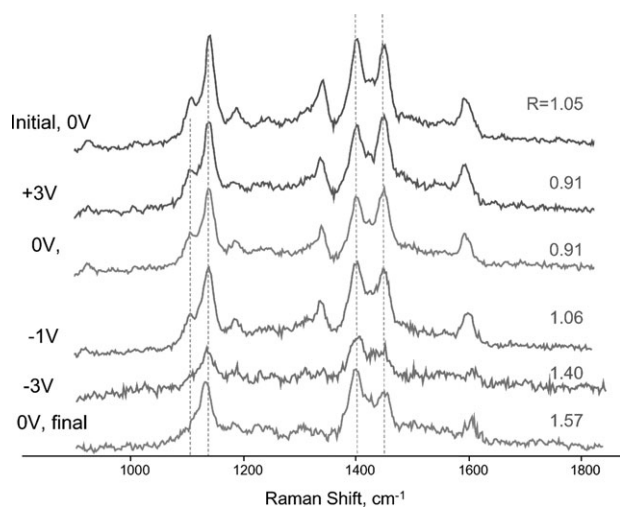


**Fig. 13** *In situ* Raman spectra of PPF/NAB(4.5)/TiO<sub>x</sub>/Au junction obtained in sequence from top to bottom, at the biases indicated on the left. R is the ratio of the 1401 : 1450 cm<sup>-1</sup> peak intensities, and a PPF spectrum was subtracted from the raw spectra in all cases. Adapted from ref. 69.

correspond to those proposed previously for electrochemical reduction of NAB.<sup>69,164</sup> As described for the case of NAB/AIO<sub>x</sub> junctions, the applied voltage causes redox reactions in the NAB which are reversible for at least several cycles. The phenyl and quinoid forms are electronically quite distinct, and would be expected to impart different electronic properties to a molecular junction. The smaller HOMO–LUMO gap in the quinoid should represent a lower tunneling barrier, as would its greater electron delocalization.<sup>66</sup> In fact, quinoid species have been invoked to explain the large conductance increase in conducting polymers upon doping to form polarons.<sup>27</sup> In the case of NAB/AIO<sub>x</sub> junctions, any electronic differences between phenyl and quinoid NAB would be minor compared to the large resistance of the AIO<sub>x</sub> layer, so no observable conductance changes accompany the NAB redox activity

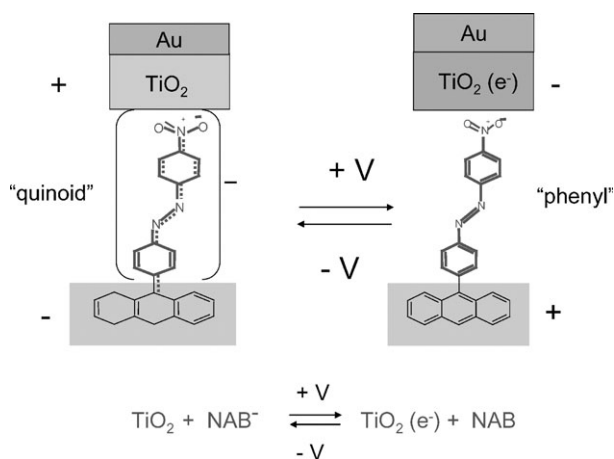


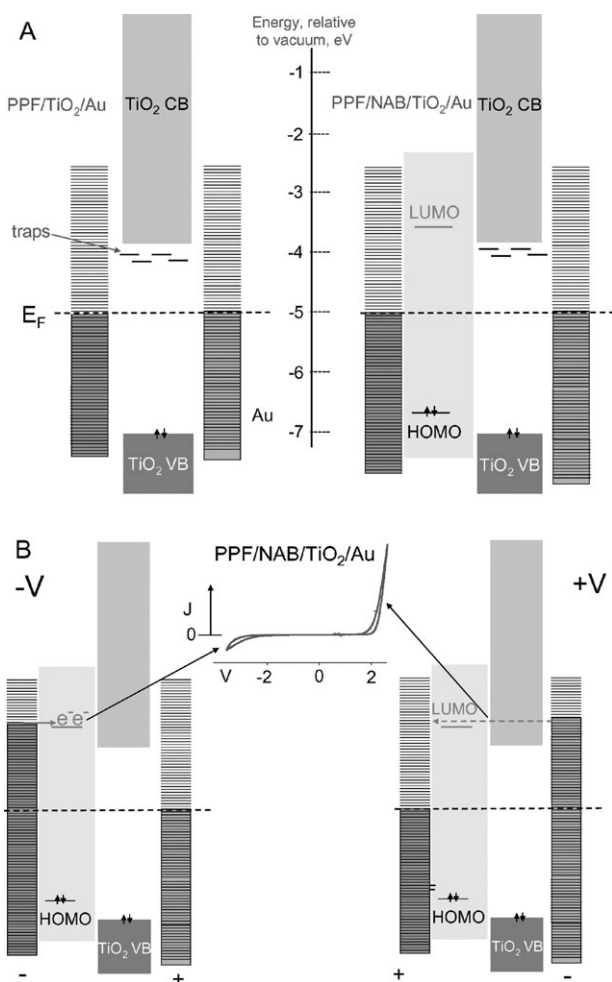
**Fig. 14** Schematic structures of redox components in PPF/NAB/TiO<sub>x</sub>/Au junctions. TiO<sub>2</sub>(e<sup>-</sup>) represents an electron in TiO<sub>2</sub> which may formally represent Ti<sup>III</sup> or Ti<sup>II</sup>. Structural details of NAB are presented in ref. 164.

observed with *in situ* Raman. However, the picture is more complex but also more interesting for the NAB/TiO<sub>x</sub> junctions, in which the oxide band gap is much smaller.

### 5.3 Bias induced conductance changes in NAB/TiO<sub>2</sub> junctions

The electronic differences between phenyl and quinoid NAB led to our proposal that conductance switching in PPF/NAB/Ti/Au junctions was caused by modulation of the redox state of the NAB.<sup>67,159</sup> The spectroscopy clearly supports the occurrence of NAB oxidation and reduction in NAB/TiO<sub>x</sub> junctions, but the strong dependence on Ti oxidation state shown in Fig. 11B equally clearly indicates that Ti oxidation is also involved in junction conductance. Consideration of the resistivities of Ti and its oxides reveals why. The resistivity of TiO<sub>2</sub> depends strongly on purity, but is approximately 10<sup>18</sup> μΩ cm at room temperature. In contrast, TiO is metallic with a resistivity (170 μΩ cm) comparable to Ti metal (42 μΩ cm). Stated differently, partial reduction of TiO<sub>2</sub> corresponds to injection of electrons into the conduction band, decreasing the oxide resistivity by as much as 15 orders of magnitude. For the 3.0 nm thick TiO<sub>x</sub> film of the present junctions, the predicted junction resistance varies from 10<sup>-11</sup> Ω cm<sup>2</sup> for pure TiO to 300 kΩ cm<sup>2</sup> for pure TiO<sub>2</sub>. The strong dependence of TiO<sub>x</sub> conductivity on oxidation state is responsible for the dramatic effects of residual gases on junction conductance illustrated in Fig. 11. An obvious corollary is that modulation of the electron density in the oxide layer of PPF/molecule/TiO<sub>2</sub>/Au junctions has a dramatic effect on junction conductance.

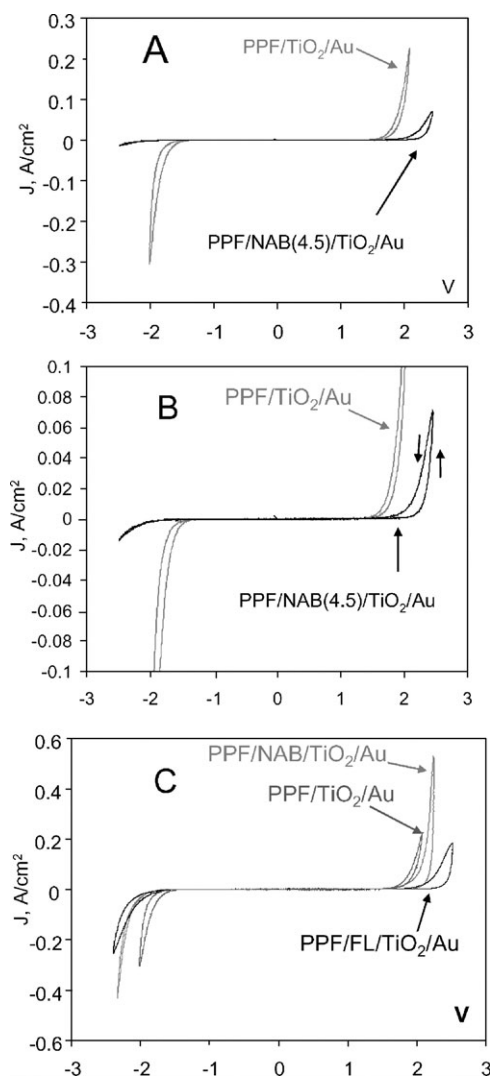
Energy level diagrams for PPF/TiO<sub>2</sub>/Au and PPF/NAB/TiO<sub>2</sub>/Au junctions are shown in Fig. 15A, with vacuum referenced energy levels for isolated materials. Given that the TiO<sub>2</sub> is deposited or formed at room temperature, it is disordered and nanocrystalline, with a presumably high density of defects. Nanocrystalline TiO<sub>x</sub> has been investigated extensively, due to its importance to dye sensitized solar cells based on TiO<sub>2</sub>. “Traps” in nanocrystalline TiO<sub>2</sub> have energies below the conduction band, and can decrease conductance in nanocrystalline TiO<sub>2</sub> by “holding” electrons below the conduction band.<sup>175–179</sup> The effect of oxidation state and traps on ET in TiO<sub>2</sub> are major subjects in their own right, but our interest here is how the electronic properties of the molecule combine with those of the TiO<sub>2</sub>. Considering first the PPF/TiO<sub>2</sub>/Au “control” junction (Fig. 12B), we see that fully oxidized TiO<sub>2</sub> has low conductance at low bias, presumably due to tunneling or defects. Based on the Simmons model for coherent tunneling<sup>73</sup> shown in Fig. 2 and a 3.0 nm thick oxide layer, the observed junctions resistance of 8600 Ω cm<sup>2</sup> for the PPF/TiO<sub>2</sub>/Au junction (Table 3) yields a calculated tunneling barrier of 1.1 eV. The agreement between this barrier height and the 1.0–1.5 eV range implied by the energy levels in Fig. 15A indicate that a coherent tunneling model is at least feasible at low bias. For higher bias ( $|V| > 2$  V) the current increases sharply, and the  $J/V$  curve is nearly symmetric about  $V = 0$ . The symmetry implies either the absence (or at least the symmetry) of significant interfacial effects (such as Schottky barriers) at the PPF/TiO<sub>2</sub> and TiO<sub>2</sub>/Au interfaces. The hysteresis apparent in Fig. 15B is likely to be a result of traps which are filled at high  $|V|$ , then emptied relatively slowly on the



**Fig. 15** A. Approximate energy level diagram for PPF/TiO<sub>2</sub>/Au and PPF/NAB/TiO<sub>2</sub>/Au junctions, relative to vacuum level. Dashed line indicates Fermi level ( $E_F$ ), and all levels are for separated materials. B. Energy levels for PPF/NAB(4.5)/TiO<sub>2</sub>/Au junction as they related to a  $J/V$  curve for the same junction.

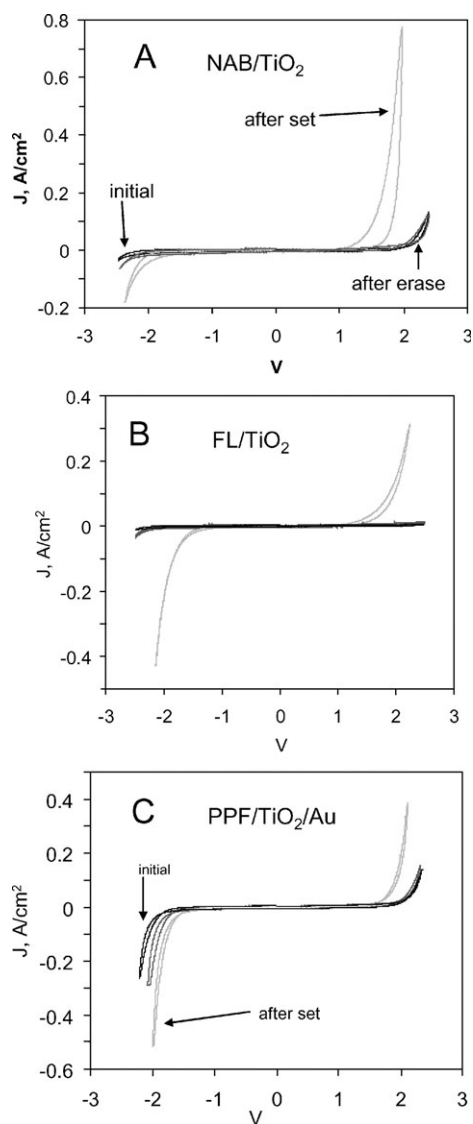
return scans. The symmetric hysteresis in the control junctions implies that electron injection and trapping are similar whether the electrons are injected from the PPF or the Au. Depending on the distribution of the electric field within the PPF/TiO<sub>2</sub>/Au junction, the increase in current for higher  $|V|$  can be viewed as nonlinear tunneling or as electron injection into the conduction band. In either case, the PPF/TiO<sub>2</sub>/Au junction behaves as a nearly symmetric metal/semiconductor/metal junction, with minimal rectification and slight but symmetric hysteresis.

Fig. 16A and B show the effect of adding a NAB multilayer (4.5 nm thick) to the 3.0 nm TiO<sub>2</sub> junction. Rectification is now pronounced, with the NAB layer causing a much greater reduction in conductance for  $V > 2$  V than for  $V < -2$  V. We proposed the scheme shown in Fig. 15B to explain rectification in NAB(4.5)/TiO<sub>2</sub>/Au junctions, based on the clear correlation between rectification and observation of NAB reduction from *in situ* Raman monitoring (Fig. 13).<sup>69,71,161</sup> The electric field across the NAB for  $V < -2$  V results in formation of the quinoid anion NAB<sup>-</sup>, generating a space charge which inhibits



**Fig. 16**  $J/V$  curves obtained at  $10 \text{ V s}^{-1}$  with 4-wire configuration for molecular junctions containing TiO<sub>2</sub> deposited from rutile in the presence of  $1 \times 10^{-5}$  Torr of O<sub>2</sub>. A. PPF/NAB(4.5)/TiO<sub>2</sub>/Au and PPF/TiO<sub>2</sub>/Au; B. same as panel A but on a more sensitive current scale; C. PPF/NAB(1.9)/TiO<sub>2</sub>/Au and PPF/FL(1.7)/TiO<sub>2</sub>/Au compared to PPF/TiO<sub>2</sub>/Au lacking a molecular layer.

ET. A slower scan rate or the presence of reduced Ti promote NAB reduction, and result in a further decrease in current density for  $V < -2$  V. The Raman spectroscopic evidence for NAB reduction at negative bias, and the resulting rectification implies formation of a significant coulomb barrier which inhibits further ET for  $V < -2$  V. For  $V > +2$  V, the positively biased NAB is oxidized to its neutral phenyl form, and electrons may traverse the NAB layer after injection through the TiO<sub>2</sub>. Charge buildup, if any, is limited to traps in the TiO<sub>2</sub>, as the NAB remains oxidized next to the positively biased PPF. The NAB layer has a relatively small effect for  $V > +2$  V, compared to TiO<sub>2</sub> alone, since the current is determined largely by electron injection through the TiO<sub>2</sub> layer. The observed conductance of the junction will depend on the energy levels of both the molecular layer and the oxide, as well as the distribution of charge and the resulting electric



**Fig. 17**  $J/V$  curves ( $1000 \text{ V s}^{-1}$ , 4-wire configuration) for PPF/molecule/ $\text{TiO}_2/\text{Au}$  junctions containing  $\text{TiO}_2$  deposited from rutile in the presence of  $1 \times 10^{-5}$  Torr of  $\text{O}_2$ . Black curves were obtained initially on a resting junction, light grey curves (red in html) were obtained after a 0.1 s pulse to +3 V, and dark grey (blue in html) curves were obtained after a 0.1 s pulse to -3 V. Panel A: PPF/NAB(1.9)/ $\text{TiO}_2/\text{Au}$ ; B: PPF/FL(1.7)/ $\text{TiO}_2/\text{Au}$ ; C: PPF/ $\text{TiO}_2/\text{Au}$ .

field through the entire structure. Nevertheless, the association of conductance changes with spectroscopically observable redox activity indicates the ability to modulate conductance by changes in the structure of the molecular and oxide layers.

As shown in Fig. 16C, and discussed previously,<sup>71</sup> the electronic behavior is different for NAB and FL monolayers compared to the NAB multilayer in  $\text{TiO}_2$  junctions. Rectification is less pronounced for NAB(1.9) and essentially absent for FL(1.7),<sup>71,161</sup> and the observed current densities are within an order of magnitude of those for  $\text{TiO}_2$  alone when the  $\text{TiO}_2$  is deposited from rutile. The  $J/V$  curves in Fig. 16C are sensitive to the degree of Ti oxidation, but the three junctions in this case were prepared identically except for the molecular layer. It would appear that there is little to distinguish the junctions

made with FL/ $\text{TiO}_2$ , NAB(1.9)/ $\text{TiO}_2$  and  $\text{TiO}_2$  alone based on the  $J/V$  responses of Fig. 16C, but as discussed in the next section, the molecular layer has pronounced effects on hysteresis and “memory”.

#### 5.4 Memory effects in PPF/molecule/ $\text{TiO}_2/\text{Au}$ junctions

We reported in 2003 on PPF/NAB (3.7)/ $\text{TiO}_x$  (50)/Au junctions, in which the degree of Ti oxidation was not well controlled.<sup>67,159</sup> When a 1 s, +4 V pulse was applied to such junctions, the conductance increased dramatically, then slowly reverted to its initial low state over a period of several minutes at zero bias. A negative potential sweep or pulse caused the high conductance state to revert rapidly to the original low value. Fig. 17 shows a similar effect in fluorene and NAB junctions in which the  $\text{TiO}_2$  was prepared from rutile in an  $\text{O}_2$  atmosphere. After an initial  $J/V$  curve was acquired, a +3 V, 0.1 s pulse was applied, another  $J/V$  curve was acquired, followed by a -3 V, 0.1 s pulse and a final  $J/V$  curve. The positive voltage pulse caused a large conductance increase which reverted back to the initial state in  $\sim 10$  min. However, the high conductance state could be “erased” rapidly with a 0.1 s pulse to -3 V. The PPF/ $\text{TiO}_2/\text{Au}$  “control” junction exhibits only a slight conductance change when the same voltage sequence is imposed (Fig. 17C), and rapidly reverts to its initial state. FL/ $\text{TiO}_2$  and NAB(1.9)/ $\text{TiO}_2$  junctions show significant and persistent changes in conductance following 0.1 s voltage pulses, as do NAB(4.5)/ $\text{TiO}_2$  junctions (not shown). The properties and mechanism of the conductance changes observed in PPF/molecule/ $\text{TiO}_2/\text{Au}$  junctions will be described in more detail elsewhere, but it is clear that both the  $\text{TiO}_2$  and molecular layer are necessary to observe the memory effect for the conditions employed, and that the rectification present in NAB(4.5) junctions is *not* a requirement to observe persistent “memory”, since NAB(1.9) and FL(1.7) junctions exhibit memory but not rectification.

The redox model proposed earlier for NAB(4.5)/ $\text{TiO}_2$  junctions has merit for explaining several aspects of the memory effect. Based on PPF/molecule/Cu junctions, we concluded that ET through thin molecular layers was fast, yielding the high current densities and low resistance apparent in Fig. 8A. For PPF/ $\text{TiO}_2/\text{Au}$  “control” junctions, transport is much slower at low bias but increases dramatically for  $|V| > 2$  V. While the PPF/ $\text{TiO}_2/\text{Au}$  junctions show some hysteresis, neither they nor PPF/molecule/Cu junctions show a significant memory effect, and both junction types have symmetric  $J/V$  curves. The addition of a molecular layer to yield PPF/molecule/ $\text{TiO}_2/\text{Au}$  makes the junction structurally asymmetric, with the consequence that carriers will traverse the molecular and  $\text{TiO}_2$  layers in different order depending on bias polarity. As noted earlier, electron injection into NAB(4.5) for negative bias causes NAB reduction and a coulomb barrier. However, a negative bias also should remove residual trapped electrons from the  $\text{TiO}_2$ , effectively oxidizing the  $\text{TiO}_2$ .<sup>69,71</sup> Whether the process is called “oxidation” of  $\text{TiO}_2$  or “detraping” of trapped electrons, the result is a shift of electron density from  $\text{TiO}_2$  to NAB under negative bias, with the resulting NAB reduction observable spectroscopically and the coulomb barrier causing rectification. Another way to

describe this response to an applied bias is to consider the redox process to be causing “dynamic doping” of the TiO<sub>2</sub>, with associated modulation of the electronic properties of the oxide.

The nearly symmetric shapes of the FL/TiO<sub>2</sub> and NAB(1.9)/TiO<sub>2</sub>  $J/V$  curves implies that the monolayers are not significantly reduced for negative bias, and do not form a coulomb barrier like NAB(4.5). However, the memory effects apparent in Fig. 17A and B indicate a persistent structural change lasting several minutes in both FL and NAB(1.9) junctions. The persistent change is nearly absent with no molecular layer and only TiO<sub>2</sub> present, but it is large and qualitatively similar for FL, NAB(1.9) and NAB(4.5) junctions containing TiO<sub>2</sub>. In order to explain the memory effect, we must propose a restructuring of the TiO<sub>2</sub> layer associated with the asymmetry imparted to the junction by the molecular layer. For negative bias, the TiO<sub>2</sub> must restructure to become less conductive, perhaps by approaching a pure TiO<sub>2</sub> composition. For positive bias, injection of electrons into the TiO<sub>2</sub> layer leads to TiO<sub>2</sub> reduction (*i.e.* “trapping”). The activation barrier for TiO<sub>2</sub> restructuring must be large enough to lead to the several minute lifetimes of the restructured states. Elements of this mechanism are admittedly speculative at present, but the correlation between redox events within the molecule/TiO<sub>x</sub> junctions and their electronic behavior is experimentally clear. In all cases examined to date, the electronic changes observed following a positive or negative bias can be explained by motion of electrons between the molecular and Ti oxide layers.

## 6. Summary and conclusions

Carbon-based molecular junctions incorporating a strong carbon-carbon bond between the substrate and molecular layer have proven to be a robust platform for investigating electron transport through molecules. Junction electronic characteristics are reproducible to approximately 20% or better, with yields above 80%. Completed junctions are stable for long periods of time, can endure temperature excursions of -150 to +100 °C, and many junction types withstand millions of  $J/V$  cycles. For the case of PPF/molecule/Cu/Au structures, the junction resistance was strongly dependent on molecular structure, ranging from 0.13 Ω cm<sup>2</sup> for NBP to 4.46 Ω cm<sup>2</sup> for BP. The weak temperature and strong thickness dependence imply a tunneling mechanism for Cu junctions, although diffusive rather than coherent tunneling is more likely for NAB and NBP multilayers with a thickness > 2.0 nm.

Junctions containing aluminium or titanium oxide have much higher resistance than the analogous Cu junctions, with electronic behavior strongly dependent on oxide composition. For PPF/NAB(4.5)/TiO<sub>x</sub>(3.0)/Au junctions the resistance ranged from 6.1 Ω cm<sup>2</sup> to 50 kΩ cm<sup>2</sup> as the oxidation state of Ti varied from primarily Ti<sup>0</sup> and Ti<sup>II</sup> to predominantly Ti<sup>IV</sup>. Accompanying this large range in resistance was progression from a symmetric  $J/V$  curve for reduced Ti to pronounced rectification for Ti<sup>IV</sup> oxide, in the case of NAB(4.5) junctions. Rectification was not observed when either the molecular layer or the oxide layer was absent, for any level for oxidation. The results are consistent with a rectification mechanism based

on reduction of NAB under negative bias to generate a coulombic barrier.

*In situ* Raman monitoring of NAB(4.5)/AlO<sub>x</sub>(3.0) and NAB(4.5)/TiO<sub>x</sub>(3.0) junctions provided strong support for the occurrence of redox reactions within molecular junctions, which are at least partially reversible for several oxidation/reduction cycles. A solid state redox reaction in a ~7.0 nm thick active layer was unexpected, but is consistent with the high electric fields across the molecular and oxide layers. For NAB and fluorene junctions containing TiO<sub>2</sub>, polarization at positive or negative bias leads to significant changes in junction conductance which persist for several minutes. Such conductance “switching” *via* a redox process could conceivably be the basis of a molecular memory device.

Two models for junction behavior which emerge from the results reported here may have general applicability to a range of molecular junctions. First, the molecule/oxide junctions may be viewed as “leaky batteries” in which the electronic conductance is a strong function of redox state. The two oppositely charged states such as those shown in Fig. 14 provide a basis for bistability, and the difference in conductance of the two states provides a means for possibly nondestructive readout of the redox state. According to this model, we expect the junction redox behavior to depend strongly on the nature and relative proportions of the various redox components present. Furthermore, the pronounced dependence of junction electronic behavior on the degree of oxidation in TiO<sub>2</sub> indicates the importance of “doping” the oxide with mobile carriers. Unlike a conventional redox cell, however, the junctions described here may not necessarily have mobile ions, and the electric fields present may be sufficient to drive redox reactions and provide charge compensation by an image charge in one or both conductors. The second general model is based on the relative electric fields across various layers and interfaces in the junction, and their effect on possible redox reactions. For fast ET through a molecular layer (*e.g.* PPF/NAB/Cu junctions) there is a small electric field, no apparent redox activity, and the  $J/V$  curve is stable for millions of cycles. With a high barrier oxide like AlO<sub>x</sub> present, however, the electric field across the molecular layer can reach several MV cm<sup>-1</sup>, leading to oxidation or reduction of the NAB. For NAB/TiO<sub>2</sub> junctions, both the NAB and TiO<sub>2</sub> are redox active, and redox activity results in observable conductance changes in response to the relatively large electric field across the junction. The reorganization in either the molecular or oxide layers associated with redox activity is presumably accompanied by an activation barrier and free energy change, which is responsible for the persistence associated with memory effects observed in PPF/molecule/TiO<sub>2</sub>/Au junctions.

## Acknowledgements

This work was supported by the National Science Foundation through project 0211693 from the Analytical and Surface Chemistry Division, and by ZettaCore, Inc. The XPS was purchased with an NSF instrumentation grant, NSF-DMR 0114098.

## References

- 1 C. A. Mirkin and M. A. Ratner, *Annu. Rev. Phys. Chem.*, 1992, **43**, 719–754.
- 2 J. Jortner and M. Ratner, *Molecular Electronics*, Blackwell Science Ltd, Oxford, 1997.
- 3 J. R. Heath and M. A. Ratner, *Phys. Today*, 2003, **56**, 43–49.
- 4 R. McCreery, *Chem. Mater.*, 2004, **16**, 4477–4496.
- 5 B. E. Bowler, A. L. Raphael and H. B. Gray, *Prog. Inorg. Chem.*, 1990, **38**, 259–322.
- 6 X. Amashukeli, N. Gruhn, D. Lichtenberger, J. Winkler and H. Gray, *J. Am. Chem. Soc.*, 2004, **126**, 15566–15571.
- 7 E. S. Krider and T. J. Meade, *J. Biol. Inorg. Chem.*, 1998, **3**, 222–225.
- 8 T. J. Meade, J. F. Kayyem and S. E. Fraser, US Pat., 5952172, 1999.
- 9 A. J. Boydston, Y. Yin and B. L. Pagenkopf, *J. Am. Chem. Soc.*, 2004, **126**, 3724–3725.
- 10 D. Segal, A. Nitzan, W. B. Davis, M. R. Wasielewski and M. A. Ratner, *J. Phys. Chem. B*, 2000, **104**, 3817–3829.
- 11 E. A. Weiss, M. J. Ahrens, L. E. Sinks, A. V. Gusev, M. A. Ratner and M. R. Wasielewski, *J. Am. Chem. Soc.*, 2004, **126**, 5577–5584.
- 12 S. Hong, R. Reifengerger, W. Tian, S. Datta, J. Henderson and C. P. Kubiak, *Superlattices Microstruct.*, 2000, **28**, 289–303.
- 13 C. J. Murphy, M. R. Arkin, Y. Jenkins, N. D. Ghatlia, S. H. Bossmann, N. J. Turro and J. K. Barton, *Science*, 1993, **262**, 1025–1029.
- 14 E. D. A. Stemp and J. K. Barton, *Met. Ions Biol. Syst.*, 1996, **33**, 325–365.
- 15 R. E. Holmlin, P. J. Dandliker and J. K. Barton, *Angew. Chem., Int. Ed. Engl.*, 1997, **36**, 2715–2730.
- 16 H. O. Finklea, in *Electroanalytical Chemistry*, ed. A. J. Bard, Dekker, New York, 1996, vol. 19, pp. 109–335.
- 17 K. S. Alleman, K. Weber and S. Creager, *J. Phys. Chem.*, 1996, **100**, 17050–17058.
- 18 S. B. Sachs, S. P. Dudek, R. P. Hsung, L. R. Sita, J. F. Smalley, M. D. Newton, S. W. Feldberg and C. E. D. Chidsey, *J. Am. Chem. Soc.*, 1997, **119**, 10563–10564.
- 19 J. J. Sumner, K. S. Weber, L. A. Hockett and S. E. Creager, *J. Phys. Chem.*, 2000, **104**, 7449–7454.
- 20 H. D. Sikes, J. F. Smalley, S. P. Dudek, A. R. Cook, M. D. Newton, C. E. D. Chidsey and S. W. Feldberg, *Science*, 2001, **291**, 1519–1523.
- 21 B. Liu, A. J. Bard, M. V. Mirkin and S. Creager, *J. Am. Chem. Soc.*, 2004, **126**, 1485–1492.
- 22 G. R. Hutchison, Y.-J. Zhao, B. Delley, A. J. Freeman, M. A. Ratner and T. J. Marks, *Phys. Rev. B: Condens. Matter*, 2003, **68**, 035204/035201–035204/035213.
- 23 Y. A. Berlin, G. R. Hutchison, P. Rempala, M. A. Ratner and J. Michl, *J. Phys. Chem. A*, 2003, **107**, 3970–3980.
- 24 J. L. Bredas, *J. Chem. Phys.*, 1985, **82**, 3808–3811.
- 25 J. Bredas, J. B. Cornil, D. Dos Santos and Z. Shuai, *Acc. Chem. Res.*, 1999, **32**, 267–276.
- 26 D. Beljonne, Z. Shuai, G. Pourtois and J. L. Bredas, *J. Phys. Chem. A*, 2001, **105**, 3899–3907.
- 27 J. L. Bredas, D. Beljonne, J. Cornil, J. P. Calbert, Z. Shuai and R. Silbey, *Synth. Met.*, 2002, **125**, 107–116.
- 28 A. Facchetti, M. Yoon, C. Stern, G. Hutchison, M. Ratner and T. Marks, *J. Am. Chem. Soc.*, 2004, **126**, 13480–13501.
- 29 J. A. Merlo, C. R. Newman, C. P. Gerlach, T. W. Kelley, D. V. Muires, S. E. Fritz, M. F. Toney and C. D. Frisbie, *J. Am. Chem. Soc.*, 2005, **127**, 3997–4009.
- 30 A. R. Murphy, J. M. J. Fréchet, P. Chang, J. Lee and V. Subramanian, *J. Am. Chem. Soc.*, 2004, **126**, 1596–1597.
- 31 P. Qi, A. Javey, M. Rolandi, Q. Wang, E. Yenilmez and H. Dai, *J. Am. Chem. Soc.*, 2004, **126**, 11774–11775.
- 32 R. Chesterfield, J. McKeen, C. Newman, P. Ewbank, D. da Silva Filho, J. Brédas, L. Miller, K. Mann and D. Frisbie, *J. Phys. Chem. B*, 2004, **108**, 19281–19292.
- 33 C. Newman, D. Frisbie, D. da Silva Filho, P. Ewbank and K. Mann, *Chem. Mater.*, 2004, **16**, 4436–4451.
- 34 S. Ando, J. Nishida, E. Fujiwara, H. Tada, Y. Inoue, S. Tokito and Y. Yamashita, *Chem. Mater.*, 2005, **17**, 1261–1264.
- 35 M. J. Panzer and C. D. Frisbie, *J. Am. Chem. Soc.*, 2005, **127**, 6960–6961.
- 36 S. N. Yaliraki, A. E. Roitberg, C. Gonzalez, V. Mujica and M. A. Ratner, *J. Phys. Chem.*, 1999, **111**, 6997–7002.
- 37 S. N. Yaliraki, M. Kemp and M. A. Ratner, *J. Am. Chem. Soc.*, 1999, **121**, 3428–3434.
- 38 M. L. Chabinyc, X. Chen, R. Holmlin, H. Jacobs, H. Skulason, C. D. Frisbie, V. Mujica, M. Ratner, M. A. Rampi and G. M. Whitesides, *J. Am. Chem. Soc.*, 2002, **124**, 11730–11736.
- 39 C. Zhou, M. R. Deshpande, M. A. Reed, L. Jones and J. M. Tour, *Appl. Phys. Lett.*, 1997, **71**, 611–613.
- 40 S. Datta, W. Tian, S. Hong, R. Reifengerger, J. I. Henderson and C. P. Kubiak, *Phys. Rev. Lett.*, 1997, **79**, 2530–2533.
- 41 T. Rakshit, G. Liang, A. Ghosh and S. Datta, *Nano Lett.*, 2004, **4**, 1803–1807.
- 42 X. Crispin, V. M. Geskin, C. Bureau, R. Lazzaroni, W. Schmickler and J. L. Bredas, *J. Chem. Phys.*, 2001, **115**, 10493–10499.
- 43 L. A. Bumm, J. J. Arnold, M. T. Cygan, T. D. Dunbar, T. P. Burgin, L. Jones, D. L. Allara, J. M. Tour and P. S. Weiss, *Science*, 1996, **271**, 1705.
- 44 Y. Xue, S. Datta, S. Hong, R. Reifengerger, J. I. Henderson and C. P. Kubiak, *Phys. Rev. B: Condens. Matter*, 1999, **59**, R7852–R7855.
- 45 Z. J. Donhauser, B. A. Mantooth, K. F. Kelly, L. A. Bumm, J. D. Monnell, J. J. Stapleton, D. W. Price, A. M. Rawlett, D. L. Allara, J. M. Tour and P. S. Weiss, *Science*, 2001, **292**, 2303–2307.
- 46 S. Howell, D. Kuila, B. Kasibhatla, C. P. Kubiak, D. Janes and R. Reifengerger, *Langmuir*, 2002, **18**, 5120–5125.
- 47 R. A. Wassel, R. R. Fuierer, N. Kim and C. B. Gorman, *Nano Lett.*, 2003, **3**, 1617–1620.
- 48 R. A. Wassel, G. M. Credo, R. R. Fuierer, D. L. Feldheim and C. B. Gorman, *J. Am. Chem. Soc.*, 2004, **126**, 295–300.
- 49 X. D. Cui, A. Primak, X. Zarate, J. Tomfohr, O. F. Sankey, A. L. Moore, T. A. Moore, D. Gust, G. Harris and S. M. Lindsay, *Science*, 2001, **294**, 571–574.
- 50 B. Xu and N. J. Tao, *Science*, 2003, **301**, 1221–1223.
- 51 F.-R. F. Fan, R. Y. Lai, J. Cornil, Y. Karzazi, J.-L. Brédas, L. Cai, L. Cheng, Y. Yao, J. David W. Price, S. M. Dirk, J. M. Tour and A. J. Bard, *J. Am. Chem. Soc.*, 2004, **126**, 2568–2573.
- 52 S. M. Lindsay, *Interface*, 2004, **13**, 26–31.
- 53 J. He, F. Chen, J. Li, O. Sankey, Y. Terazono, C. Herrero, D. Gust, T. Moore, A. L. Moore and S. M. Lindsay, *J. Am. Chem. Soc.*, 2005, **127**, 1384–1385.
- 54 F.-R. F. Fan, J. Yang, L. Cai, D. W. Price, S. M. Dirk, D. Kosynkin, Y. Yao, A. M. Rawlett, J. M. Tour and A. J. Bard, *J. Am. Chem. Soc.*, 2002, **124**, 5550–5560.
- 55 F.-R. F. Fan, Y. Yao, L. Cai, L. Cheng, J. M. Tour and A. J. Bard, *J. Am. Chem. Soc.*, 2004, **126**, 4035–4042.
- 56 J. Chen, L. C. Calvet, M. A. Reed, D. W. Carr, D. S. Grubisha and D. W. Bennett, *Chem. Phys. Lett.*, 1999, **313**, 741–748.
- 57 C. P. Collier, G. Matternsteig, E. W. Wong, Y. Luo, K. Beverly, J. Sampaio, F. M. Raymo, J. F. Stoddart and J. R. Heath, *Science*, 2000, **289**, 1172–1175.
- 58 M. A. Reed and J. M. Tour, *Sci. Am.*, 2000, 86–93.
- 59 M. A. Reed, J. Chen, A. M. Rawlett, D. W. Price and J. M. Tour, *Appl. Phys. Lett.*, 2001, **78**, 3735–3737.
- 60 C. P. Collier, J. O. Jeppesen, Y. Luo, J. Perkins, E. W. Wong, J. R. Heath and J. F. Stoddart, *J. Am. Chem. Soc.*, 2001, **123**, 12632–12641.
- 61 A. R. Pease, J. O. Jeppesen, J. F. Stoddart, Y. Luo, C. P. Collier and J. R. Heath, *Acc. Chem. Res.*, 2001, **34**, 433–444.
- 62 J. Chen, M. A. Reed, A. M. Rawlett and J. M. Tour, *Science*, 1999, **286**, 1550–1552.
- 63 N. A. Melosh, A. Boukai, F. Diana, B. Gerardot, A. Badolato, P. M. Petroff and J. R. Heath, *Science*, 2003, **300**, 112–115.
- 64 S. Ranganathan, I. Steidel, F. Anariba and R. L. McCreery, *Nano Lett.*, 2001, **1**, 491–494.
- 65 F. Anariba and R. L. McCreery, *J. Phys. Chem. B*, 2002, **106**, 10355–10362.
- 66 A. O. Solak, S. Ranganathan, T. Itoh and R. L. McCreery, *Electrochem. Solid-State Lett.*, 2002, **5**, E43–E46.
- 67 R. L. McCreery, J. Dieringer, A. O. Solak, B. Snyder, A. Nowak, W. R. McGovern and S. DuVall, *J. Am. Chem. Soc.*, 2003, **125**, 10748–10758.
- 68 R. McCreery, *Interface*, 2004, **13**, 46–51.

- 69 A. Nowak and R. McCreery, *J. Am. Chem. Soc.*, 2004, **126**, 16621–16631.
- 70 F. Anariba, J. Steach and R. McCreery, *J. Phys. Chem. B*, 2005, **109**, 11163–11172.
- 71 R. P. Kalakodimi, A. Nowak and R. L. McCreery, *Chem. Mater.*, 2005, **17**, 4939–4948.
- 72 D. R. Lamb, *Electrical Conduction Mechanisms in Thin Insulating Films*, Methuen and Co., London, 1968.
- 73 J. G. Simmons, *DC Conduction in Thin Films*, Mills and Boon Ltd, London, 1971.
- 74 A. Nitzan and M. A. Ratner, *Science*, 2003, **300**, 1384–1389.
- 75 V. Mujica and M. A. Ratner, *Chem. Phys.*, 2001, **264**, 365–370.
- 76 M. D. Newton, *Theor. Chem. Acc.*, 2003, **110**, 307–321.
- 77 X.-Q. Li, H. Zhang and Y. Yan, *J. Phys. Chem. A*, 2001, **105**, 9563–9567.
- 78 M. Galperin, D. Segal and A. Nitzan, *J. Chem. Phys.*, 1999, **111**, 1569–1579.
- 79 M. Abu-Hilu and U. Peskin, *Chem. Phys.*, 2004, **296**, 231–241.
- 80 W. B. Davis, W. A. Svec, M. A. Ratner and M. R. Wasielewski, *Nature*, 1998, **396**, 60–63.
- 81 K. Weber, L. Hockett and S. Creager, *J. Phys. Chem. B*, 1997, **101**, 8286–8291.
- 82 S. Creager, C. J. Yu, C. Bamdad, S. O'Connor, T. MacLean, E. Lam, Y. Chong, G. T. Olsen, J. Luo, M. Gozin and J. F. Kayyem, *J. Am. Chem. Soc.*, 1999, **121**, 1059–1064.
- 83 J. F. Smalley, H. O. Finkea, C. E. D. Chidsey, M. R. Linfood, S. E. Creager, J. P. Ferraris, K. Chalfant, T. Zawodzinski, S. W. Feldberg and M. D. Newton, *J. Am. Chem. Soc.*, 2003, **125**, 2004–2013.
- 84 S. M. Sze, *The Physics of Semiconductor Devices*, Wiley, New York, 2nd edn, 1981.
- 85 C. S. Sosnoff, M. Sullivan and R. W. Murray, *J. Phys. Chem.*, 1994, **98**, 13643–13650.
- 86 N. A. Surridge, C. S. Sosnoff, R. Schmehl, J. S. Facci and R. W. Murray, *J. Phys. Chem.*, 1994, **98**, 917–923.
- 87 R. H. Terrill, P. E. Sheehan, V. C. Long, S. Washburn and R. W. Murray, *J. Phys. Chem.*, 1994, **98**, 5127–5134.
- 88 R. H. Terrill and R. W. Murray, in *Molecular Electronics*, ed. J. Jortner and M. Ratner, Blackwell Science Ltd, Oxford, 1997, pp. 215–239.
- 89 S. Ranganathan and R. Murray, *J. Phys. Chem. B*, 2004, **108**, 19982–19989.
- 90 F. C. Grozema, Y. A. Berlin and L. D. A. Siebbeles, *J. Am. Chem. Soc.*, 2000, **122**, 10903–10909.
- 91 M. Bixon and J. Jortner, *J. Am. Chem. Soc.*, 2001, **123**, 12556–12567.
- 92 A. J. Epstein, W. P. Lee and V. N. Prigodin, *Synth. Met.*, 2001, **117**, 9–13.
- 93 D. A. Buttry and F. C. Anson, *J. Am. Chem. Soc.*, 1983, **105**, 685–689.
- 94 C. E. D. Chidsey and R. W. Murray, *Science*, 1986, **231**, 25–31.
- 95 L. Geng, R. A. Reed, M.-H. Kim, T. T. Wooster, B. N. Oliver, J. Egekeze, R. T. Kennedy, J. W. Jorgenson, J. F. Parger and R. W. Murray, *J. Am. Chem. Soc.*, 1989, **111**, 1614–1619.
- 96 N. A. Surridge, M. E. Zvanuf, F. R. Keene, S. C. Sosnoff, M. Silver and R. W. Murray, *J. Phys. Chem.*, 1992, **96**, 962–970.
- 97 D. Segal, A. Nitzan, M. A. Ratner and W. D. Davis, *J. Phys. Chem. B*, 2000, **104**, 2790–2793.
- 98 J. R. Heath, *Acc. Chem. Res.*, 1999, **32**, 388.
- 99 R. M. Metzger, *Acc. Chem. Res.*, 1999, **32**, 950.
- 100 R. M. Metzger, *Chem. Rev.*, 2003, **103**, 3803.
- 101 R. M. Metzger, J. W. Baldwin, W. J. Shumate, I. R. Peterson, P. Mani, G. J. Mankey, T. Morris, G. Szulcowski, S. Bosi, M. Prato, A. Comito and Y. Rubin, *J. Phys. Chem. B*, 2003, **107**, 1021–1027.
- 102 R. G. Nuzzo and D. L. Allara, *J. Am. Chem. Soc.*, 1983, **105**, 4481.
- 103 M. D. Porter, T. B. Bright, D. L. Allara and C. E. D. Chidsey, *J. Am. Chem. Soc.*, 1987, **109**, 3559–3568.
- 104 K. Konstadinidis, P. Zhang, R. L. Opila and D. L. Allara, *Surf. Sci.*, 1995, **338**, 300–312.
- 105 Y. Selzer, M. A. Cabassi, T. S. Mayer and D. L. Allara, *J. Am. Chem. Soc.*, 2004, **126**, 4052–4053.
- 106 J. C. Love, L. A. Estroff, J. K. Kriebel, R. G. Nuzzo and G. M. Whitesides, *Chem. Rev.*, 2005, **105**, 1103–1170.
- 107 A. Balakumar, A. B. Lysenko, C. Carcel, V. L. Malinovskii, D. T. Gryko, K. H. Schweikart, R. S. Loewe, A. A. Yasserli, Z. M. Liu, D. F. Bocian and J. S. Lindsey, *J. Org. Chem.*, 2004, **69**, 1435–1443.
- 108 L. Wei, D. Syomin, R. Loewe, J. Lindsey, F. Zaera and D. Bocian, *J. Phys. Chem. B*, 2005, **109**, 6323–6330.
- 109 P. T. Hurley, A. E. Ribbe and J. M. Buriak, *J. Am. Chem. Soc.*, 2003, **125**, 11334–11339.
- 110 J. Buriak, *Chem. Rev.*, 2002, **102**, 1272–1308.
- 111 E. G. Robins, M. P. Stewart and J. M. Buriak, *Chem. Commun.*, 1999, 2479–2480.
- 112 C. A. Richter, C. A. Hacker and L. J. Richter, *J. Phys. Chem. B*, 2005, **109**, 21836–21841.
- 113 C. A. Hacker, K. A. Anderson, L. J. Richter and C. A. Richter, *Langmuir*, 2005, **21**, 882–889.
- 114 S. Lefant, C. Krzeminski, C. Delerue, G. Allan and D. Vuillaume, *Nano Lett.*, 2003, **3**, 741–746.
- 115 D. F. Padowitz and R. J. Hamers, *J. Phys. Chem. B*, 1998, **102**, 8541–8545.
- 116 R. J. Hamers, S. K. Coulter, M. D. Ellison, J. S. Hovis, D. F. Padowitz, M. P. Schwartz, C. M. Greenlief and J. N. Russell, Jr, *Acc. Chem. Res.*, 2000, **33**, 617–624.
- 117 M. Delamar, R. Hitmi, J. Pinson and J. M. Saveant, *J. Am. Chem. Soc.*, 1992, **114**, 5883–5884.
- 118 P. Allongue, M. Delamar, B. Desbat, O. Fagebaume, R. Hitmi, J. Pinson and J. M. Saveant, *J. Am. Chem. Soc.*, 1997, **119**, 201–207.
- 119 M. Delamar, G. Desarmot, O. Fagebaume, R. Hitmi, J. Pinson and J. M. Saveant, *Carbon*, 1997, **35**, 801–807.
- 120 A. Adenier, M.-C. Bernard, M. M. Chehimi, E. Cabet-Deliry, B. Desbat, O. Fagebaume, J. Pinson and F. Podvorica, *J. Am. Chem. Soc.*, 2001, **123**, 4541–4549.
- 121 M.-C. Bernard, A. Chausse, E. Cabet-Deliry, M. M. Chehimi, J. Pinson, F. Podvorica and C. Vautrin-UI, *Chem. Mater.*, 2003, **15**, 3450–3462.
- 122 A. Adenier, E. Cabet-Deliry, A. Chaussé, S. Griveau, F. Mercier, J. Pinson and C. Vautrin-UI, *Chem. Mater.*, 2005, **17**, 491–501.
- 123 J. Pinson and F. Podvorica, *Chem. Soc. Rev.*, 2005, **34**, 429–439.
- 124 Y.-C. Liu and R. L. McCreery, *J. Am. Chem. Soc.*, 1995, **117**, 11254.
- 125 F. Anariba, S. H. DuVall and R. L. McCreery, *Anal. Chem.*, 2003, **75**, 3837–3844.
- 126 C. Saby, B. Ortiz, G. Y. Champagne and D. Belanger, *Langmuir*, 1997, **13**, 6805–6813.
- 127 B. Ortiz, C. Saby, G. Y. Champagne and D. Belanger, *J. Electroanal. Chem.*, 1998, **455**, 75–81.
- 128 T.-C. Kuo, R. L. McCreery and G. M. Swain, *Electrochem. Solid-State Lett.*, 1999, **2**, 288–291.
- 129 S. Ranganathan, R. L. McCreery, S. M. Majji and M. Madou, *J. Electrochem. Soc.*, 2000, **147**, 277–282.
- 130 S. Ranganathan and R. L. McCreery, *Anal. Chem.*, 2001, **73**, 893–900.
- 131 W. Yang, O. Auciello, J. E. Butler, W. Cai, J. Carlisle, J. Gerbi, D. Gruen, T. Knickerbocker, T. Lasseter, J. John N. Russell, L. M. Smith and R. J. Hamers, *Nat. Mater.*, 2002, **1**, 253–257.
- 132 T. Knickerbocker, T. Strother, M. P. Schwartz, J. N. Russell Jr, J. Butler, L. M. Smith and R. J. Hamers, *Langmuir*, 2003, **19**, 1938–1942.
- 133 T. Lasseter, B. Clare, N. Abbott and R. J. Hamers, *J. Am. Chem. Soc.*, 2004, **126**, 10220–10221.
- 134 K.-Y. Tse, B. M. Nichols, W. Yang, J. E. Butler, J. N. Russell, Jr, and R. J. Hamers, *J. Phys. Chem. B*, 2005, **109**, 8523–8532.
- 135 Y.-C. Liu and R. L. McCreery, *Anal. Chem.*, 1997, **69**, 2091.
- 136 J. K. Kariuki and M. T. McDermott, *Langmuir*, 1999, **15**, 6534–6540.
- 137 J. K. Kariuki and M. T. McDermott, *Langmuir*, 2001, **17**, 5947–5951.
- 138 M. S. Strano, C. A. Dyke, M. L. Usrey, P. W. Barone, M. J. Allen, H. Shan, C. Kittrell, R. H. Hauge, J. M. Tour and R. E. Smalley, *Science*, 2003, **301**, 1519–1522.
- 139 J. L. Bahr, J. Yang, D. V. Kosynkin, M. J. Bronikowski, R. E. Smalley and J. M. Tour, *J. Am. Chem. Soc.*, 2001, **123**, 6536–6542.
- 140 C. Combellas, F. Kanoufi, J. Pinson and F. Podvorica, *Langmuir*, 2005, **21**, 280–286.

- 141 R. Kostecki, X. Song and K. Kinoshita, *Electrochem. Solid-State Lett.*, 1999, **2**, 465.
- 142 R. Kostecki, B. Schnyder, D. Allia, X. Song, K. Kinoshita and R. Kotz, *Thin Solid Films*, 2001, **396**, 36–43.
- 143 S. Ranganathan, PhD Thesis, The Ohio State University, 2001.
- 144 I. L. Spain, in *Chemistry and Physics of Carbon*, ed. P. L. Thriver, Dekker, New York, 1981, vol. 16, pp. 119–304.
- 145 R. L. McCreery, in *Electroanalytical Chemistry*, ed. A. J. Bard, Dekker, NY, 1991, vol. 17, pp. 221–374.
- 146 A. M. Nowak and R. L. McCreery, *Anal. Chem.*, 2004, **76**, 1089–1097.
- 147 F. Anariba, U. Vishwanathan, D. Bocian and R. McCreery, *Anal. Chem.*, 2006, **78**, 3104–3112.
- 148 G. L. Fisher, A. Hooper, R. L. Opila, D. R. Jung, D. L. Allara and N. Winograd, *J. Electron Spectrosc. Relat. Phenom.*, 1999, **98–99**, 139–148.
- 149 G. L. Fisher, A. E. Hooper, R. L. Opila, D. R. Jung, D. L. Allara and N. Winograd, *J. Phys. Chem. B*, 2000, **104**, 3267–3273.
- 150 G. L. Fisher, A. V. Walker, A. E. Hooper, T. B. Tighe, K. B. Bahnck, H. T. Skriba, M. D. Reinard, B. C. Haynie, R. L. Opila, N. Winograd and D. L. Allara, *J. Am. Chem. Soc.*, 2002, **124**, 5528–5541.
- 151 B. C. Haynie, A. V. Walker, T. B. Tighe, D. L. Allara and N. Winograd, *Appl. Surf. Sci.*, 2003, **203–204**, 433–436.
- 152 A. V. Walker, T. B. Tighe, B. C. Haynie, S. Uppili, N. Winograd and D. Allara, *J. Phys. Chem. B*, 2005, **109**, 11263–11272.
- 153 B. d. Boer, M. M. Frank, Y. J. Chabal, W. Jiang, E. Garfunkel and Z. Bao, *Langmuir*, 2004, **20**, 1539–1542.
- 154 R. Haag, M. A. Rampi, R. E. Holmlin and G. M. Whitesides, *J. Am. Chem. Soc.*, 1999, **121**, 7895–7906.
- 155 K. Slowinski, K. U. Slowinska and M. Majda, *J. Phys. Chem. B*, 1999, **103**, 8544–8551.
- 156 K. Slowinski and M. Majda, *J. Electroanal. Chem.*, 2000, **491**, 139–147.
- 157 R. E. Holmlin, R. Haag, M. L. Chabynyc, R. F. Ismagilov, A. E. Cohen, A. Terfort, M. A. Rampi and G. M. Whitesides, *J. Am. Chem. Soc.*, 2001, **123**, 5075–5085.
- 158 C. P. Collier, E. W. Wong, M. Belohradsky, F. M. Raymo, J. F. Stoddart, P. J. Kuekes, R. S. Williams and J. R. Heath, *Science*, 1999, **285**, 391–394.
- 159 R. McCreery, J. Dieringer, A. O. Solak, B. Snyder, A. M. Nowak, W. R. McGovern and S. DuVall, *J. Am. Chem. Soc.*, 2004, **126**, 6200.
- 160 W. R. McGovern, F. Anariba and R. McCreery, *J. Electrochem. Soc.*, 2005, **152**, E176–E183.
- 161 R. McCreery, U. Vishwanathan, R. J. Kalakodimi and A. M. Nowak, *Faraday Discuss.*, 2006, **131**, 33–43.
- 162 A. N. Pullen, PhD Dissertation, Ohio State University, 2004.
- 163 W. R. McGovern, PhD Dissertation, Ohio State University, 2005.
- 164 T. Itoh and R. L. McCreery, *J. Am. Chem. Soc.*, 2002, **124**, 10894–10902.
- 165 S. Datta, *Electronic Transport in Mesoscopic Systems*, Cambridge University Press, Cambridge, 1995.
- 166 A. V. Ghosh, T. Rakshit and S. Datta, *Nano Lett.*, 2004, **4**, 565–568.
- 167 W. Wang, T. Lee and M. Reed, *J. Phys. Chem. B*, 2004, **108**, 18398–18407.
- 168 C. Kergueris, J. P. Bourgoin, S. Palacin, D. Esteve, C. Urbina, M. Magoga and C. Joachim, *Phys. Rev. B: Condens. Matter*, 1999, **59**, 12505.
- 169 C. Joachim, *Superlattices Microstruct.*, 2000, **28**, 305–315.
- 170 L. Grill, K.-H. Rieder, F. Moresco, S. Stojkovic, A. Gourdon and C. Joachim, *Nano Lett.*, 2005, **5**, 859–863.
- 171 Moth-Poulsen, K. L. Patrone, N. Stuhr-Hansen, J. B. Christensen, J.-P. Bourgoin and T. Bjornholm, *Nano Lett.*, 2005, **5**, 783–785.
- 172 B. Chen and R. M. Metzger, *J. Phys. Chem.*, 1999, **103**, 4447–4451.
- 173 D.R. Stewart, D. A. A. Ohlberg, P. A. Beck, Y. Chen, R. S. Williams, J. O. Jeppesen, K. A. Nielsen and J. F. Stoddart, *Nano Lett.*, 2004, **4**, 133–136.
- 174 D. Mardare, C. Baban, R. Gavrilu, M. Modreanu and G. I. Rusu, *Surf. Sci.*, 2002, **507–510**, 468–472.
- 175 S. Leytner and J. T. Hupp, *Chem. Phys. Lett.*, 2000, **330**, 231–236.
- 176 D. Kuciauskas, M. S. Freund, H. B. Gray, J. R. Winkler and N. S. Lewis, *J. Phys. Chem. B*, 2001, **105**, 392–403.
- 177 J. Nelson, A. M. Eppler and I. M. Ballard, *J. Photochem. Photobiol., A*, 2002, **148**, 25–31.
- 178 M. Bailes, P. J. Cameron, K. Lobato and L. M. Peter, *J. Phys. Chem. B*, 2005, **109**, 15429–15435.
- 179 V. Mikhelashvili and G. Eisenstein, *J. Appl. Phys.*, 2001, **89**, 3256–3269.